The Pennsylvania State University
The Graduate School

FLIGHT PATH PLANNING OF UAV BASED ON ATMOSPHERIC ENERGY HARVESTING

A Thesis in
Aerospace Engineering
by
Anjan Chakrabarty

© 2010 Anjan Chakrabarty

Submitted in Partial Fulfillment
of the Requirements
for the Degree of

Master of Science

August 2010

The thesis of Anjan Chakrabarty was reviewed and approved* by the following:

Jacob W Langelaan
Assistant Professor of Aerospace Engineering
Thesis Advisor

Mark D. Maughmer
Professor of Aerospace Engineering

George A. Lesieutre
Professor of Aerospace Engineering
Head of the Department of Aerospace Engineering

*Signatures are on file in the Graduate School.

Abstract

This thesis presents an approach to planning long distance soaring trajectories which exploit atmospheric energy to enable long distance, long duration flights by small and micro unmanned aerial vehicles. It introduces the energy map, which computes the minimum total energy required to reach the goal from an arbitrary starting point while accounting for the effect of arbitrary wind fields. The energy map provides the path to the goal as a sequence of way points, the optimal speeds to fly for each segment between way points and the heading required to fly along a segment. Since the energy map is based on the minimum total energy required to reach the goal it immediately answers the question of existence of a feasible solution for a particular starting point and initial total energy.

The results obtained from energy map are compared with other generic trajectory planners, namely A*. The A* algorithm used uses a cost function which is the weighted sum of energy required and remaining distance to goal. The effect of varying the weight parameter on the flight paths is examined. The energy expended along a path for varying weight is examined, and the results are compared with a wavefront expansion planning algorithm. The weight is selected based on maximum energy utilization that is available from the atmosphere and minimizing time to reach the goal. Optimal weight is selected based on simulation results.

Both the methods of path planning are now used in real wind field data. Energy efficient routes are found in the real wind field using both the methods.

Table of Contents

List of Figures

List of Tables

Acknowledgments

The work presented in this thesis would not have been possible without guidance and constant encouragement from a lot of people. I would like to take this opportunity to express my gratitude to some of the individuals who have helped me all the way.

First of all I would like to thank my advisor Dr. Jack Langelaan for giving me the opportunity to work in this interesting topic. His insight of looking into a difficult problem from a practical point of view has helped me to gain significant insights towards solving the problem.

I would like to thank Dr. Mark D. Maughmer for reviewing the thesis and providing helpful intellectual insights.

I am also grateful towards my friends for constant help and support. Particularly I would like to thank Sean Quinn Marlow who's helpful insights have always been there whenever I needed them. I would also like to thank Shane Tierney , Nathan Depenbusch and Sana Sarfraz for creating an atmosphere in the lab which was both fruitful and enjoyable.

I am proud that I was born to parents who have inculcated within me the quest for knowledge the indomitable desire to know. Growing up with my brother was both fun and educative. My brother is my friend philosopher and guide. Constant encouragements form my family have always been my forte.

Dedication

Dedicated to my parents

Dedication

Chapter 1

Introduction

This thesis presents path planning through complex wind fields based on energy harvesting from the atmosphere. The motivation of this research is to enable Small Uninhabited Aerial Vehicles (UAVs, here "small" means hand-launchable) being capable of long distance long range operations. Small UAVs are limited in range and endurance because of their limitation of fuel that can be carried on board. Moreover, the best L/D attainable for small UAVs is typically much smaller than for larger aircraft. While improvements in battery technology will enable longer duration missions, immediate performance improvements can achieved by harvesting energy available from the atmosphere.

Graph based path planning has been successfully applied for path planning in mobile robots. Graph based path planning methods are used for identifying energy efficient routes in the environment. Graph based planning problem poses certain problems. Firstly the continuous space has to be discretized in such a manner such that there is no loss of information. Moreover one has to explicitly define discrete cost of transition through the graph. Moreover information about the world has to be known *a priori*.

The thesis will:

- provide a mathematical framework for energy harvesting through any arbitrary wind field.
- Introduce a new concept in planning where the solution itself will provide intuitive understanding about the feasibility of paths

- Use known planning algorithms modified for this application of energy harvesting.
- Present simulation results to demonstrate the effectiveness of using the methods for energy harvesting.
- Finally use the techniques to find energy efficient routes in the environment.

1.1 Motivation

Birds constantly use atmospheric energy to minimize energy required for their travel. Indeed, large birds such as hawks (Figure 1.1a)and eagles as well as human sailplane and hang glider pilots (Figure 1.1b) routinely exploit the energy available from updrafts of air to fly for hundreds of kilometers without flapping wings or the use of engines. Migratory birds follow certain routes while traversing there journey to a distant goal. They all use energy available from the atmosphere. For this kind of long range paths updrafts is the main source from which energy can be harvested.

(a) Red-tailed hawk (*Buteo jamaicensis*). This bird is widespread throughout North America. Image source: www.richard-seaman.com.

(b) Gliders using ridge soaring for long distance travel. Image Source: http://en.wikipedia.org/wiki/File:RidgeSrn.gif

Figure 1.1. Practical applications where wind energy is used for long distance travel.

Updrafts have three main causes: uneven heating of the ground, which produces buoyant instabilities known as thermals; long period oscillations of the atmosphere,

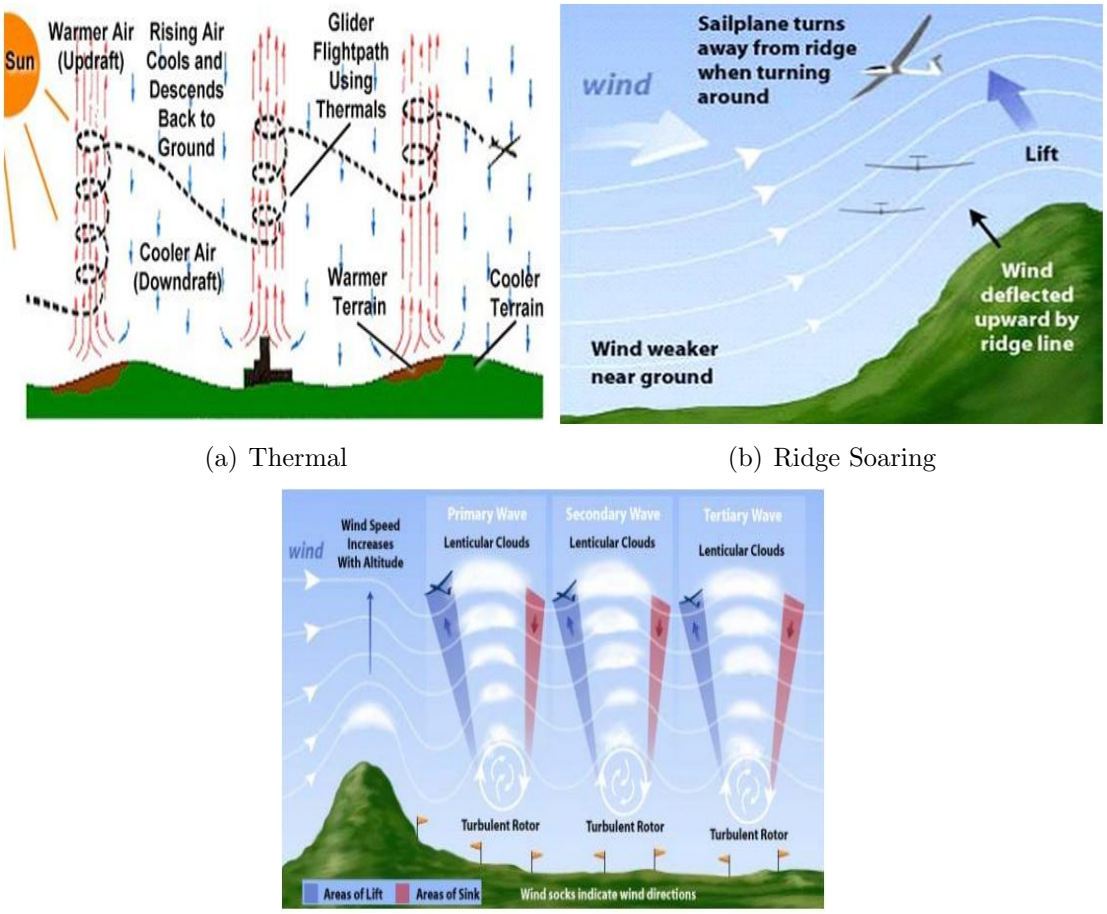

(a) Thermal

(b) Ridge Soaring

(c) Wave

Figure 1.2. Different types of updrafts used for static soaring. Image source: http://www.aerospaceweb.org/question/nature/q0253.shtml

generally called wave, which occurs in the lee of large mountain ranges; and orographic lift, where wind is deflected by the slopes of hills and mountains. Typically updrafts have life spans measured in minutes (for thermals) to hours or days (for ridge and wave lift). Ridge lift and wave are predictable phenomena, and thus one can use trajectory planning techniques to compute paths which exploit vertical air motion to enable extremely long distance or duration flights.

A second means of extracting energy from the air uses velocity gradients (which can occur near the ground due to the boundary layer) or shear layers (which often occur on the leeward side of mountains and ridges). This strategy, called dynamic soaring, was first described by Lord Rayleigh in an analysis of albatross flight [1, 2]. Dynamic soaring is again becoming the subject of research both for recreational

flight (mainly by RC flying enthusiasts) and for UAV flight. However, this class of dynamic soaring generally requires highly agile flight in close proximity to the ground: this is a very risky endeavor.

The third means of extracting energy from the air exploits gusts. It has been observed that the flight performance of large birds is improved by gusts, while it is typically reduced on human-piloted aircraft [3]. This suggests that birds are able to extract energy from gusts, and indeed Kiceniuk reports that it is even possible to extract energy from a downward gust [4]! Extracting energy from gusts is complicated by their typically short duration, hence very fast response (typically exceeding human reaction time) is required. Control laws have been developed to enable energy extraction from gusts by small UAVs [5].

These three methods of extracting energy from the environment can be used to enable autonomous long duration, long distance (denoted by $(LD)^2$ flight) for unmanned air vehicles. These three methods of extracting energy are referred to as static soaring, dynamic soaring and gust soaring respectively.

The major focus of the thesis is is utilizing static soaring for enabling long endurance and long range flight. Paths will be planned according to minimum energy utilization and maximum energy available from the atmosphere.

1.2 Related Work

A rich and varied literature exists in the field of optimal static soaring trajectories with the application of human-piloted soaring flight.

Autonomous static soaring is now becoming the focus of more research. Simulation results of thermal flight are reported by Allen (2005) [6] and flight test results are presented in Allen (2007) [7]. Edwards reports very impressive results of autonomous thermal soaring [8]. However, these do not consider the problem of trajectory planning.

Wind routing for powered aircraft has been considered for both crewed and uncrewed aircraft. Rubio describes a planning method based on genetic algorithms [9]; Jardin discusses a method based on neighborhood optimal control [10]. Neither of these approaches consider the possibility of harvesting energy from vertical components of the wind field. Several authors have addressed the optimal static

soaring trajectory problem in the context of soaring competition. The MacCready problem [11, 12], the final glide problem [13], and "Dolphin" flight along regions of alternating lift and sink [14, 15, 16] all address optimal static soaring including optimal speed to fly between thermals of known strength. de Jong [17] describes a geometric approach to trajectory optimization. Most of this research is limited by known lift distribution (e.g. sinusoidally varying lift [18] or "square wave" lift [19]) and generally do not consider the effects of horizontal wind components.

Recent works including simulation results of thermal flight are reported by Allen (2005) [6] and flight test results are presented in Allen (2007) [7]. Autonomous thermal soaring has has also been addressed by Edwards [8]. However, because thermals are unpredictable trajectory planning is not addressed.

A genetic algorithm approach to flight path planning wind has been addressed by Rubio [9]. Jardin uses neighboring optimal control [10] for wind routing problems. But none of these approaches uses the fact that energy can be harvested in regions of upward moving air.

The focus of this thesis is on planning long-distance soaring trajectories which harvest energy available from a known wind field (this may be obtained from predictions generated using meteorological forecasting tools such as MM5 [20]). Previous research addressed this problem using a probabilistic road map approach [21] and using a gradient-based optimization [22].

Path planning methods are widely used in robotics application. The concept of configuration space was first introduced by Lozano-Perez and Wesley [23], [24]. The planning in the configuration space is typically approached using one of the three methods: search based, sampling based or a combination of both. Search based methods are most widely used in the field of robotics owing to its ease of implementation. The idea behind search based planning us simply to search a regularly sized grid cell which represents the configuration space. The first algorithm was Dijkstra's which was a variant of depth first algorithm [25]. In 1968 the A* algorithm was introduced where the search procedure was narrowed by introduction of a Heuristic. A* is a complete search algorithm, i.e it will find a path if one exists, but A* is a static algorithm.

For path planning in soaring application an wavefront expansion approach from the goal is taken. This method is compared with the A* method where the cost

function for A* contains energy gains from the atmosphere.

1.3 System Overview

Autonomous soaring is a complex problem. Moreover graphs based techniques are used to identify energetically favorable routes in the environment. The environment will first be discretized by placing nodes or way points. It is assumed that the wind information is known at each node. Using kinematics a mathematical model is proposed which minimizes energy loss over a segment. It will be shown that only velocity and thrust coefficient will completely describe the input to the vehicle. The heading will be dictated by the nodes that the vehicle will fly. The cost to fly between two nodes will be calculated.

In the first case this energy is minimized only with the restriction that the vehicle has to always fly towards the goal. Thus energy required at each point in the environment to reach the goal is found. Paths are obtained from tracing back from the goal the start point. This is an upper bound on the minimum energy to reach the goal.

In the second case the restriction of always flying to the goal is removed and transition to all the neighboring nodes are allowed. A* algorithm is used where the cost function is a linear combination of energy expended in the transition and remaining distance to goal.

Both the methods are used in real wind field data.

1.4 Contributions

The major contribution of the thesis are outlined below.

- **Path Planning Based on energy Map** A new method have been developed for path planning based on wave front expansion. It is called the Energy Map. The Energy map is the minimum energy that the aircraft should have to make it to the goal with the constraint of always flying to the goal.

- **Path Planning Based on A* algorithm** Paths planned by the energy map approach are compared with A* paths where the constraint of always moving to the goal is removed and the cost function is a linear combination of energy harvested from the atmosphere and the distance to the goal.

- **Routes of Minimum Energy in Real Wind Data** real wind field data is used to detect minimum energy routes by both the methods.

1.5 Readers Guide

The reminder of the thesis is organized is follows

- **Chapter 2** describes the energy harvesting problem mathematically. Minimizing energy over a segment is discussed and the cost function associated with graph based planning is detailed.

- **Chapter 3** describes how graph based solutions are used to solve this kind of problems. A single destination shortest path problem aka the Energy map is discussed and the performance of energy map is sample wind fields are performed.

- **Chapter 4** defines how heuristic search procedures can be used for soaring application. An useful cost function is found through simulations in different wind cases.

- **Chapter 5** original wind data obtained from the Meteorological Department of Central Pennsylvania. The two different methods are tested in this wind data and energy effienct rouotes are determined in given wind field.

- **Chapter 6** presents the concluding remarks and future works.

Chapter 2

The Planning Problem

The following chapter defines the path planning problem based on energy harvesting from the atmosphere. The major topics discussed are

1. Problem Statement: The setup of the path planning problem is described. Discretization of the environment is detailed and graph based path planning is proposed for flight path planning.

2. Kinematics and Energetics of Soaring Flight: A mathematical model is derived for the kinematics of soaring flight. Different cases for minimizing energy required for flight between two particular nodes with arbitrary wind is discussed

3. Graph Based Path Planning: Different graph based path planning techniques are introduced and why certain other graph based techniques cannot be used in this application is discussed.

2.1 Problem Statement

The problem considered here is a given a certain wind field what is the best path to the goal utilizing maximum energy from the environment. Energy is available from the vertical component of wind (i.e updrafts). It is assumed that *a priori* information about the wind field is available (this may be obtained from predictions generated using meteorological forecasting tools such as MM5). Graph based tech-

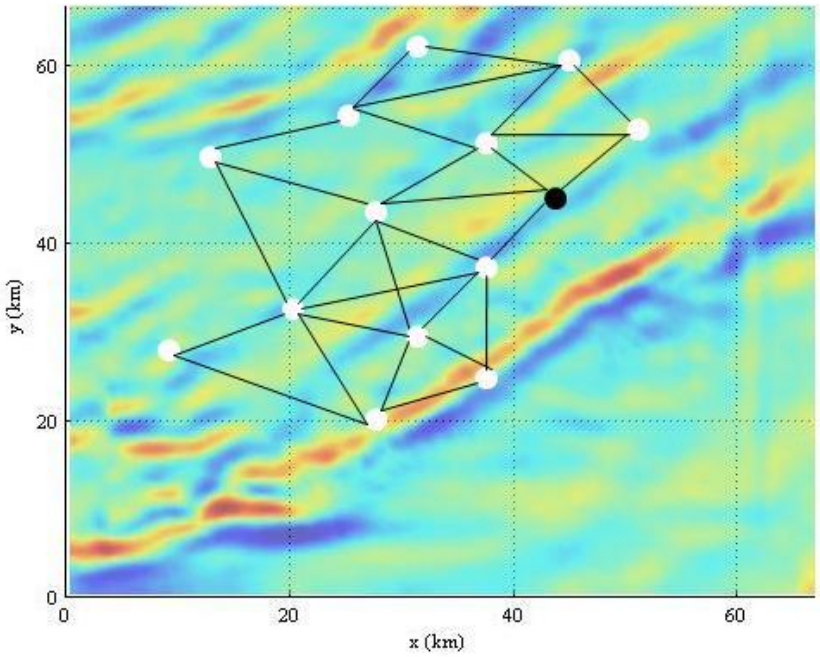

Figure 2.1. Schematic of graph-based planning for autonomous soaring over a wind field.

niques have been successfully implemented in many robotic application for path planning. The robot's configuration space is divided into finite number of regions (or nodes), and the planning problem is reduced to finding a sequence of of neighboring nodes between the start and goal nodes(e.g. Stentz [26]). These graph-based techniques have been used very successfully in many wheeled ground robot path planning problems and have been used for some UAV planning problems, typically radar evasion [27]. However, these techniques typically only consider a fixed cost for a transition between nodes in a graph (e.g. time required) and vehicle speed is kept constant. In aircraft applications total energy can be a critical parameter in trajectory planning (for example, when considering the fuel required to reach the goal). Both environmental and control parameters can affect the energy required for a particular transition: a head wind will increase the required total energy, as will flying at non-optimal airspeed. Thus any graph-based planning technique will require a means of accounting for environmental and control conditions in the analysis of costs of transitions between nodes or cells.

Figure 2.1 shows a schematic of graph based planning applied to autonomous soaring. Contours show the vertical component of wind, with red showing upward motion (allowing energy harvesting) and blue showing downward motion. The environment is first seeded with waypoints (or nodes) and edges. This set of nodes $i = \{i = 0 \dots m\}$ (with $i = 0$ denoting the goal) and edges $ij = \{i = 0 \dots m, j = 0 \dots m\}$ connecting nodes define the allowable paths to the goal. Each edge ij is assigned a constant wind vector $\mathbf{w}_{ij}$ with components $w_{x,ij}$, $w_{y,ij}$, and $w_{z,ij}$. Wind field information is assumed to be available *a priori*. Figure 2.1 shows a sample grid where the set of nodes are generated randomly. The black dot is the goal node and the white dots are randomly placed nodes to discretize the environment. The line segment joining two nodes are the edges. Here the energy required to complete a transition forms a major part of the cost function of a transition. Note that the energy e_{ij} required to complete a transition from node i to node j is not necessarily the same as e_{ji}. Once the graph has been defined a minimum cost path can be found between any two nodes.

2.1.1 Minimum energy paths

The minimum total energy required to complete each of the transitions in the graph (note that the energy e_{ij} required to complete a transition from node i to node j is not necessarily the same as e_{ji}) has to be calculated. The trajectory planning problem then becomes a problem of finding the minimum energy path through the digraph to the goal, i.e. the sequence of nodes $\mathbf{n}$ which minimizes the energy required to reach the goal

$$e_{goal} = \sum_{i \in \mathbf{n}, j \in \mathbf{n}} e_{ij} \tag{2.1}$$

Several techniques have been developed to compute cost-minimizing paths through a graph. Dijkstra's Algorithm is not applicable here because it is restricted to problems where edge costs are non-negative, and the Bellman-Ford algorithm encounters problems when negative cycles exist [28]. In this application a non-negative edge cost implies energy gain, which occurs with flight through an updraft of sufficient strength. Negative energy cycles occur when the aircraft flies

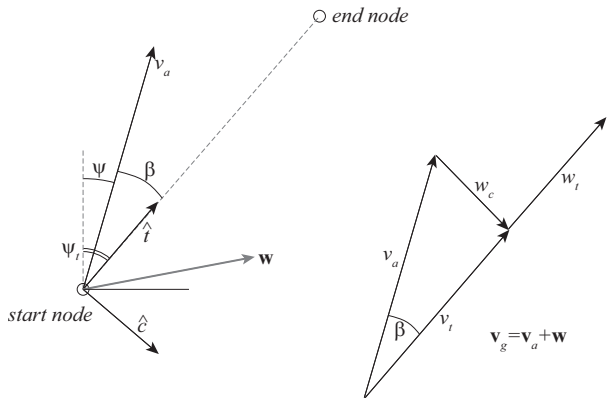

Figure 2.2. Track coordinate frames (left) and resolution of airspeed and wind vectors into the track coordinate frame (right).

repeatedly between two nodes, gaining energy with each trip.

The path planning problem is thus composed of:

- **Defining the distribution of nodes and edges.** Ideally the node distribution will account for changes in wind field, with higher density in regions of rapidly changing wind.
- **Determining costs for each edge.** This involves computing the cost of transition along each edge in the graph. Here energy expended is the main contributor to this cost.
- **Finding a minimum cost path through the graph.**

The problem of node distribution is not discussed in this thesis. Regular (but not necessarily uniform) Cartesian grids are used here.

2.2 Flight between two nodes

The first part of determining the cost of transition is defining the kinematics of flight between two neighboring nodes. Referring to Figure 2.2 the line segment joining two successive nodes is the desired ground track. The velocity of the vehicle is decomposed into in-track v_t and cross track v_c components, hence to maintain flight along the desired ground track $v_c = 0$. The wind vector is also decomposed

into in-track w_t and cross-track w_c components. v_g is the ground speed of the vehicle.

From Figure 2.2 the relationship between air speed, ground speed, heading and ground track for an arbitrary horizontal component of wind can be obtained:

$$v_t = \sqrt{v_a^2 \cos^2\gamma - w_c^2} \tag{2.2}$$

$$v_g = v_t + w_t \tag{2.3}$$

$$v_a \cos\gamma \sin\beta = w_c \tag{2.4}$$

where v_g is the magnitude of the ground speed, $v_a \cos\gamma$ is the projection of the airspeed vector onto the horizontal plane and β is the angle between the airspeed vector and the desired ground track. Recall that flight path angle γ is assumed to be small, hence $\cos\gamma \approx 1$ and the ground speed is $v_g \approx \sqrt{v_a^2 - w_c^2} + w_t$. The constraint $v_c = 0$ is expressed in Equation 2.4.

The aircraft heading to maintain the desired ground track is $\psi = \psi_t - \beta$. Hence

$$\psi = \psi_t - \sin^{-1}\frac{w_c}{v_a} \tag{2.5}$$

Clearly heading ψ is dependent on airspeed v_a. The problem now is to determine the optimal value of airspeed v_a and thrust coefficient C_T for flight between two nodes. This will be done by analyzing the energy required to fly the path segment between the nodes.

2.3 Vehicle Kinematics and Energetics

It is assumed that an on-board controller is able to follow heading, airspeed and throttle commands. Moreover, it is assumed that response to step changes in commands is very fast compared with the duration of a particular command. Hence a point mass model is sufficient to describe vehicle motion for planning purposes (Figure 2.3). Vehicle kinematics are given by

$$\dot{x} = v_a \cos\gamma \cos\psi + w_x \tag{2.6}$$

$$\dot{y} = v_a \cos\gamma \sin\psi + w_y \tag{2.7}$$

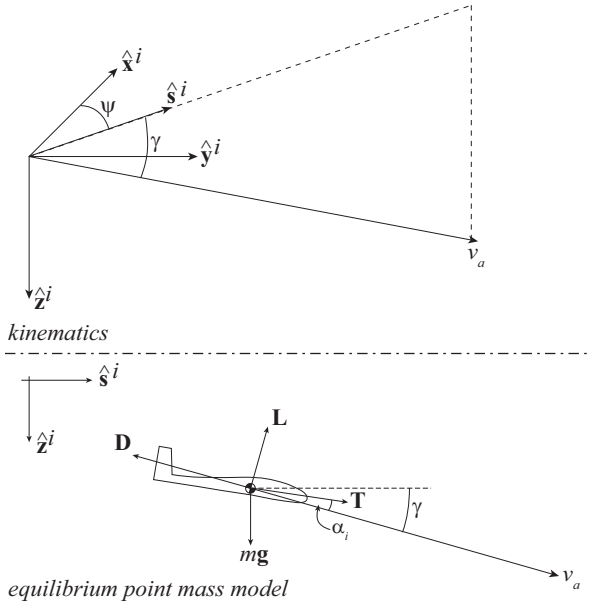

Figure 2.3. Point mass model.

$$\dot{z} = v_a \sin\gamma + w_z \tag{2.8}$$

where v_a is airspeed, γ is flight path angle with respect to the surrounding airmass, ψ is heading and w_x, w_y and w_z are the three components of the 3D wind vector.

The flight path angle γ is a function of airspeed v_a and throttle setting T, and can be obtained for steady flight. From (Figure 2.3) resolving forces parallel and perpendicular to the flight path,

$$mg\cos\gamma = L + T\sin\alpha \tag{2.9}$$

$$mg\sin\gamma = D - T\cos\alpha \tag{2.10}$$

where m is mass of the vehicle and α is the angle of attack (NB this implicitly assumes that the thrust axis is aligned with the aircraft's body-x axis). Using the standard definition of force coefficients,

$$\cos\gamma = \frac{qS}{mg}\left(C_L + C_T\sin\alpha\right) \tag{2.11}$$

$$\sin\gamma = \frac{qS}{mg}\left(C_D - C_T\cos\alpha\right) \tag{2.12}$$

where C_L and C_D are lift and drag coefficient, q is the dynamic pressure, S is the wing area, g is gravitational acceleration constant.

It is assumed that the flight path angle γ is small, hence $\sin\gamma \approx \gamma$ and $\cos\gamma \approx 1$. During trimmed cruise flight angle of attack is generally small (3° to 6°) and thrust is significantly smaller in magnitude than lift. Hence it is further assumed that $C_T \sin\alpha$ is negligible compared with C_L. From Equation 2.11

$$C_L = \frac{mg}{qS} = \frac{2mg}{\rho v_a^2 S} \tag{2.13}$$

Here C_L is lift coefficient, ρ is density of the air, and S is wing area. A polynomial approximation is used for the aircraft's drag polar:

$$C_D = \sum_{i=0}^{n} a_i C_L^i \tag{2.14}$$

Typically a second order polynomial is used to represent drag coefficient. However, this is often only valid over a fairly narrow speed range, and here a fourth order polynomial is used.

Substituting into Equation 2.12, the air mass relative flight path angle for a particular speed and thrust can thus be computed as

$$\sin\gamma = \frac{qS}{mg}\left(\sum_{i=0}^{n} a_i C_L^i - C_T\right) \tag{2.15}$$

Combining Equation 2.13 with Equation 2.15 and vehicle kinematics, the vehicle's flight path is completely specified by inputs $\mathbf{u} = [v_a \ \psi \ C_T]^T$ and wind speed $\mathbf{w}$. This model is adequate as long as the length of time of each trajectory segment is large compared with the time constant of the vehicle's step response with respect to the inputs $\mathbf{u}$.

The inputs v_a and C_T affects the energy expended during the flight, thus the choice of input is critical to energy efficient flight.

2.4 Minimizing Energy Loss

Using the kinematics defined earlier the steady state airspeed which minimizes the energy lost over a segment (or equivalently, maximizes the energy gained) will be determined. Total energy is

$$E_{tot} = mgh + \frac{m}{2}v_a^2 + E_s \tag{2.16}$$

where h is altitude and E_s is on-board stored energy. Specific total energy is

$$\begin{aligned} e_{tot} = \frac{E_{tot}}{mg} &= h + \frac{v_a^2}{2g} + \frac{E_s}{mg} \\ &= h + \frac{v_a^2}{2g} + e_s \end{aligned} \tag{2.17}$$

Minimizing energy lost over a segment means maximizing $\frac{\Delta e_{tot}}{\Delta s}$. In steady state flight this is equivalent to maximizing $\frac{\dot{e}}{v_g}$, in other words flying to maximize range. The rate of change of specific energy is

$$\dot{e}_{tot} = \dot{h} + \frac{v_a \dot{v}_a}{g} + \dot{e}_s \tag{2.18}$$

In steady flight acceleration is zero, hence

$$\dot{e}_{tot} = \dot{h} + \dot{e}_s = -\dot{z} + \dot{e}_s \tag{2.19}$$

Recall that z is positive down and $\dot{z}$ is defined in Equation 2.8.

The quantity $\dot{e}_s$ is the rate of change of on-board stored energy. This is dependent on motor power and the efficiency of energy conversion.

$$\dot{e}_s = -\frac{T v_a}{mg\eta_{ec}\eta_p} = -\frac{qS}{mg}\frac{C_T v_a}{\eta_{ec}\eta_p} \tag{2.20}$$

where η_{ec} is the net efficiency of energy conversion from source to shaft (in electrical power systems this is the product of motor efficiency and speed controller efficiency) and η_p is the propeller efficiency.

Thus the rate of change of total energy (in steady state flight) is

$$\dot{e}_{tot} = -(v_a \sin\gamma + w_z) - \frac{qS}{mg}\frac{C_T v_a}{\eta_{ec}\eta_p} \tag{2.21}$$

and maximum range flight occurs when one maximizes

$$\frac{\dot{e}_{tot}}{v_g} = -\frac{v_a \sin\gamma + w_z}{\sqrt{v_a^2 - w_c^2} + w_t} - \frac{qS}{mg}\frac{C_T v_a}{\eta_{ec}\eta_p\left(\sqrt{v_a^2 - w_c^2} + w_t\right)} \tag{2.22}$$

There may be cases where on-board energy is especially valuable (for example, to maximize time on station at the goal). In this case a reward function which weights stored energy more heavily may be appropriate.

$$r_e = \frac{\dot{h}}{v_g} + \mu\frac{\dot{e}_s}{v_g} \tag{2.23}$$

Here setting $\mu > 1$ will increase the importance of conserving on-board energy.

Hence the problem is to find the airspeed v_a and throttle setting C_T which solves the optimization problem

$$\begin{aligned}
\text{maximize} \quad & \frac{\dot{h}}{v_g} + \frac{\dot{e}_s}{v_g} && (2.24)\\
\text{subject to} \quad & \dot{h} = -v_a \sin\gamma - w_z && (2.25)\\
& v_g = \sqrt{v_a^2 - w_c^2} + w_t && (2.26)\\
& \sin\gamma = \frac{qS}{mg}\left(\sum_{i=0}^{n} a_i C_L^i - C_T\right) && (2.27)\\
& v_{a,min} \le v_a \le v_{a,max} && (2.28)\\
& C_{T,min} \le C_T \le C_{T,max} && (2.29)\\
& v_g > 0 && (2.30)
\end{aligned}$$

The constraint defined by Equation 2.27 defines the air mass relative flight path angle. Equation 2.26 and Equation 2.30 together ensure that the vehicle always proceeds forward along the desired ground track. Airspeed limits are defined by Equation 2.28 and thrust coefficient limits are defined by Equation 2.29

Since e has dimension distance, $\frac{\dot{e}}{v_g}$ is a dimensionless quantity. Equation 2.13

and Equation 2.15 together show that flight path angle with respect to air is a function of airspeed and throttle setting (because in trimmed flight C_L is a function of airspeed). Hence for flight paths $\frac{\dot{e}}{v_g}$ is a function only of airspeed and thrust coefficient, and the airspeed and thrust coefficient which maximizes energy gained over a segment can be computed. Note that in zero wind the energy change is always negative.

Under certain conditions additional constraints may exist (e.g. gliding flight, constant altitude flight). Constraints such as altitude limits can also be added as needed.

2.4.1 Gliding flight

For gliding flight $C_T = 0$ and $\dot{e}_s = 0$. The only free control input for flight along a path segment is airspeed, and the optimization problem is

$$\text{maximize} \quad \frac{-(v_a \sin\gamma + w_z)}{\sqrt{v_a^2 - w_c^2} + w_t} \tag{2.31}$$

$$\text{subject to} \quad \sin\gamma = \frac{qS}{mg}\sum_{i=0}^{n} a_i C_L^i \tag{2.32}$$

$$C_L = \frac{mg}{qS} \tag{2.33}$$

$$v_{a,min} \leq v_a \leq v_{a,max} \tag{2.34}$$

$$v_g > 0 \tag{2.35}$$

This effectively minimizes the flight path angle with respect to the ground, and if upwards component of wind is large enough the earth relative flight path angle will be negative. The constraints of equation Equation 2.32 and Equation 2.33 define steady state flight.

In zero wind this will result in flight at best L/D.

2.4.2 Constant altitude flight

Many missions include altitude restrictions (for example to ensure separation or to ensure appropriate sensor coverage). Hence aircraft motion will be restricted to constant altitude. This has the additional benefit of reducing graph size (since

there is no need to discretize in the vertical direction), improving computational feasibility.

At constant altitude $\dot{h} = 0$. Hence $v_a \sin\gamma = -w_z$:

$$\sin\gamma = \frac{qS}{mg}\left(\sum_{i=0}^{n} a_i C_L^i - C_T\right) = -\frac{w_z}{v_a} \tag{2.36}$$

and the optimization problem becomes

$$\text{maximize} \quad \frac{\dot{e}_s}{v_g} \tag{2.37}$$

$$\text{subject to} \quad \frac{qS}{mg}\left(\sum_{i=0}^{n} a_i C_L^i - C_T\right) = -\frac{w_z}{v_a} \tag{2.38}$$

$$v_g = \sqrt{v_a^2 - w_c^2} + w_t \tag{2.39}$$

$$v_{a,min} \leq v_a \leq v_{a,max} \tag{2.40}$$

$$C_{T,min} \leq C_T \leq C_{T,max} \tag{2.41}$$

$$v_g > 0 \tag{2.42}$$

The constraint defined by Equation 2.38 limits the vehicle to constant altitude flight. Equation 2.39 and Equation 2.42 together ensure that the vehicle always proceeds forward along the desired ground track. Airspeed limits are defined by Equation 2.40 and thrust coefficient limits are defined by Equation 2.41.

Thus this constraint will ensure that the vehicle will fly in constant altitude and $\frac{\dot{e}_s}{v_g}$ will be maximized by increasing either the kinetic energy or by minimizing energy expenditure.

2.5 Regenerative Soaring

For battery powered aircraft a wind milling propeller (or a ram air turbine) can be used to recharge batteries at the cost of increased drag. One can thus trade potential energy (altitude) for stored electrical energy. When flying through a strong enough updraft it is possible to either:

- gain potential energy by climbing at constant speed

- gain kinetic energy by flying at higher speed but at constant altitude
- gain stored electrical energy by flying at constant speed and altitude and windmilling the propeller.

Of course a combination of the three can also occur.

Using a windmilling propeller to gain electrical energy is known as regenerative soaring, and was first described by MacCready. [29]

In the context of the optimization problem posed above, setting $C_{T,min} = 0$ means that regeneration cannot occur (as $\dot{e}_s$, the energy expended from the on-board supply, has a minimum value of zero). Permitting negative values of $C_{T,min}$ implies that $\dot{e}_s$ can be positive quantity (Equation 2.20), and thus the energy (potential and/or kinetic) can be transferred to batteries.

For constant altitude flight $\dot{e}_s$ signifies cost of transition between two nodes. Energy expenditure $\dot{e}_s$ will in general be positive, i.e, energy is required to make a certain transition. Thus $\dot{e}_s < 0$ means negative energy expenditure or gaining energy from the atmosphere which can be stored by charging the batteries. There is a limit to the amount to which the batteries can be charged. Thus regenerative soaring is allowed up to the full capacity of the batteries and once the batteries have been fully charged $C_{T,min}$ is set to zero.

2.6 Cost Of Transition between Nodes

The energy required to fly a segment of the flight path can thus be found using the approach discussed above. This can now be used to define the cost of a transition in the graph which is used to discretize the planning problem. The cost of a transition is defined as

$$c_{ij} = -\frac{\dot{e}}{v_g}\bigg|_{ij,opt} \tag{2.43}$$

i.e. the energy expended in a transition. A generic function minimizer (such as MatLab's `fmincon`) can be used to find v_a^{opt} and C_T^{opt} which minimizes c_{ij} while ensuring that constraints such as airspeed limits (stall and maximum speed) are not exceeded. Once v_a^{opt} has been computed the required heading to maintain the

desired ground track between the start and end nodes is computed from Equation 2.27.Recall that in the optimization problem defined above, the change in energy for a flight segment is maximized. The optimal energy *cost* of a transition is thus the negative of this optimal energy change. The procedure outlined above is used to find the minimum energy loss c^*_{ij}, optimal airspeed v_a^{opt} and required heading to fly the desired ground track for each of the allowable transitions in the environment. Once the cost of transition have been defined a graph based approach can be used to find minimum cost paths through the environment.

2.7 Examples of Optimal Velocity and Thrust Coefficient for SB-XC glider

For the rest of the thesis calculations were performed for an RnR Products SB-XC glider; parameters are given in Appendix A. This section will provide some intuitive understanding of various parameters that are calculated in the different section.

Based on optimization criteria in the previous section for different wind cases the optimal speeds and and optimal thrust coefficient for the SB-XC glider are calculated. In all the cases the aircraft is constraint to flight at constant altitude which is used in flight path planning.

Table 2.1. Optimal Speed and Thrust Coefficient for SB-XC glider.

wind	v_a^{opt}	C_T^{opt}
Zero wind	15.8 m/s	0.0238
Upward wind of 1m/s with regeneration	14.6 m/s	-0.0228
Upward wind of 1m/s without regeneration	21.6 m/s	0
Downward wind of 1m/s	20.8 m/s	0.0342
Headwind 1m/s	15.9 m/s	0.0234
Tailwind 1m/s	15.7 m/s	0.0242

It can be seen from Table 2.1 at zero wind condition for minimum energy expenditure the aircraft flies at best L/D and the the velocity of the aircraft at best L/D is 15.8 m/s. In upwards moving air the aircraft either flies faster (thus

increasing kinetic energy) if regeneration is not allowed or flies with negative thrust coefficient (recharging batteries) if regeneration is allowed. While moving through downward wind the velocity increase to reduce the time over which downward air motion affects the aircraft. A tail wind results in an airspeed below best L/D in still air and a headwind results in flight at an airspeed greater than best L/D in still air.

2.8 Graph Based Path Planning

Graph based planning methods are extensively used for mobile robots trajectory planning. Path planning methods transform a continuous problem (ie, finding a path to a distant goal) into a discrete problem of searching a graph between initial node and goal node. The goal is to find a "shortest" path from the start to the goal. The "shortest" path will be based on the discrimination of the cost [30].

2.8.1 Single Source Shortest Path(SSSP)

The shortest path problem is the problem of finding a path between two vertices (or nodes) to minimize the sum of weights of the individual edges. The environment is first seeded with nodes with a weighted directed graph. The weight functions being real valued weights. Edge weights can represent time, cost ,penalties, loss or any other quantity that accumulates linearly along a path that one wants to minimize. In this particular case the energy required for each transition forms the most important part of the cost function. Note that the energy required $e_{i,j}$ required to complete the transition from node i to j is not necessarily same as the energy required for transition from j to i (headwind becomes a tail wind). Further, in some cases energy can be harvested along a transition (e.g. when flying through an updraft), leading to a negative transition cost. The cost can also be a linear combination of one or two of the individual costs that are described, eg. a linear combination of either of energy expended, distance, time.

There are many variants of SSSP.

1. Single-Destination shortest path problem

2. Single-pair shortest path problem

3. All pair shortest path problem.

In single destination shortest path shortest path is found to a given destination from each vertex. If this problem is solved one also solves the Single pair shortest path problem. The all pair shortest path problem is not considered here. Most robotic application requires single pair shortest path problems. There are plenty of known algorithms of solving single pair shortest path problems.

Because of the presence of negative transition cost, as the aircraft can gain energy from updrafts Dijkstra's algorithm is thus not applicable here. Further, negative cycles are likely to exist (e.g. when the aircraft flies repeatedly through an updraft, gaining energy with each cycle). Hence the Bellman-Ford algorithm cannot be directly applied [28].

Finding the *shortest path* between the start and goal node will be answered in this thesis with two different flavors. First a single destination shortest path approach is taken. Thus shortest path to the goal from all nodes of the domain are calculated. This method not only provides a possible path to the goal, but also computes the minimum energy required to reach the goal from anywhere in the domain. This is an important criteria because this will enable one for feasibility of flights between two certain points in the environment.

Another approach for solving the *shortest path* will be answered using A* algorithm. A* is a classical algorithm [Hart, Nilsson and Raphael,1968] [Nilsson,1980]. Under simple conditions A* is guaranteed to return a path of minimum cost whenever a path exists, and to return a failure otherwise. In this particular case the feasibility of such paths will be checked based on energy requiremnets and time constraints.

A careful comparison is made between both the methods and both the methods are tested against real wind field data.

2.9 Summary

This chapter has defined the use of graph based techniques to solve the path planning problem defined by energy constraints. The section of kinematics and energetics has given an insight into the equations of motion and what is being optimizing to maximize energy gained from the atmosphere. Optimal speed and

thrust coefficients for SB-XC glider through different wind conditions are calculated. Finally how graph based techniques can be used for solving these kinds of problems have been discussed.The two distinct methods of solutions are discussed in the next chapters. The success of Graph based techniques have been exploited to be used in soaring applications. The next chapter will demonstrate single source shortest path techniques to effectively plan in presence of arbitrary wind in order to minimize energy expenditure of the batteries.

Chapter 3

The Energy Map

In this chapter graph based planning techniques has be implemented in planning soaring trajectories. A variant of Single destination shortest path problem has been devised which is hence forth referred to as *energy map*.

3.1 Introduction

Recall that standard graph search algorithms such as Dijksta's Algorithm and Bellman-Ford Algorithm cannot be directly applied to the problem of autonomous soaring. However, adding constraints can allow the problem to be solved. To remove problems associated with cycles one can add constraints: e.g. A* only allows a node to be visited once. Another approach is to constrain transitions so they are always towards the goal. This is a rather severe constraint, however it enables very fast computation of minimum energy paths to the goal through wavefront expansion.

This wavefront expansion method allows the definition of a map which specifies the minimum energy required to reach a goal from anywhere in the environment. This map (denoted by *energy map*) actually defines an upper bound on the minimum energy required to reach the goal: the constraint of transitions towards the goal means that a lower-energy path may actually exists. However the energy map can immediately answer the question of existence of a feasible path to the goal: if a vehicle begins with higher energy than that defined by the energy map, then it is guranteed to have a feasible path to the goal.

3.1.1 Map Definition and Minimum Energy Paths

To define the energy map, the environment is first seeded with waypoints (or nodes) and edges. This set of nodes $i = \{i = 0 \dots m\}$ (with $i = 0$ denoting the goal) and edges $ij = \{i = 0 \dots m, j = 0 \dots m\}$ connecting nodes define the allowable paths to the goal. Each edge ij is assigned a constant wind vector $\mathbf{w}_{ij}$ with components $w_{x,ij}$, $w_{y,ij}$, and $w_{z,ij}$. Wind field information is assumed to be available a priori.

After the set of nodes and the set of allowable transitions has been defined, the cost of each transition is computed. In steady state flight, the energy e_{ij} required to fly from node i to j is a function of the wind vector $\mathbf{w}_{ij}$, air speed v_a and throttle setting T. The heading ψ_{ij} required to fly along the desired ground track between the two nodes is a function of the horizontal component of the wind field and the air speed. The problem of computing v_a which minimizes the energy required for transition ij is discussed in Section 2.3.

It is assumed that the vehicle is in a trimmed, steady state condition during each transition over an edge ij, and the time required to change from one trim condition to the next as a node is passed is short compared with the length of time required to complete a transition.

Aside from the constraint that the time required to complete a transition at a particular trim condition is long compared with the time required to change trim conditions from one transition to the next (which defines the minimum node spacing), node placement is arbitrary. Higher node density can thus be used in regions where spatial gradients in wind field are large, allowing higher resolution trajectories when necessary.

3.1.2 Minimum Energy Paths via Wavefront Expansion

An example discretization is shown in Figure 3.1. The goal is shown as the black circle and allowable transitions are shown as a black circle and allowable transitions are shown as arrows. To generate the energy map, the set of nodes is first ordered by increasing distance to goal, and transitions which simultaneously satisfy the condition of being to a neighboring node and reducing the distance to the goal are defined as allowable.

The energy to reach the goal is computed for the group of nodes nearest the

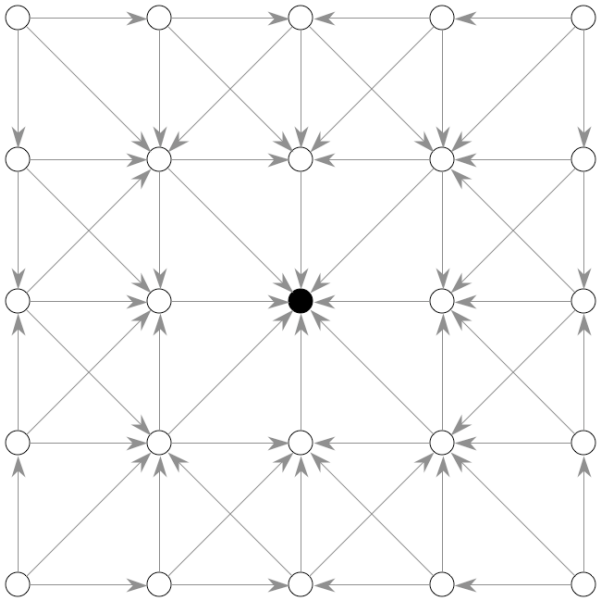

Figure 3.1. Sample regular Cartesian grid showing allowable transitions for wavefront expansion. The goal is at the center of the grid.

goal, and the energy corresponding to each node is defined as their respective costs-to-go. For the next group of nodes the energy required to reach nearest neighbors in the first group is computed, and the cost-to-go for each node is the minimum total energy over all possible paths to the goal. The process continues until energy to goal has been computed for each node. This is a breadth-first dynamic programming approach, and with the constraint that transitions must always end in nodes nearer to the goal, the resulting energy map gives an upper bound on the minimum energy required to reach the goal from any point in the environment.

In this approach each node is encoded with the total energy required to reach the goal (i.e. the cost to go), the next node in the path to the goal, and the control inputs (speed to fly and heading) required to reach the next node. The energy map thus encodes a complete path to the goal from anywhere in the environment. Further, it provides a means to check the feasibility of a path to the goal for an aircraft with a particular initial position and initial total energy.

Note that paths found using this method are not necessarily minimum energy approaches: since paths are constrained to always approach the goal, trajectories which are more energy efficient may exist. Such a path would first proceed

away from the goal before turning towards it. However, relaxing the constraint that the goal must be approached would make the wave front expansion approach computationally intractable for large environments.

A critical criterion in hardware implementation is the time required to compute a solution. Fast planning solutions permit on-line re-planning as changes in the environment (i.e. the wind field) occur. Here, the definition of nodes and the allowable transitions between nodes is pre-determined and stored in a tree. Computing the costs of allowable transitions and maintaining the minimum cost to go for each node can thus be performed quickly.

3.2 Energy Maps for Horizontal Wind Fields

To demonstrate the energy mapping approach energy maps for some simple wind fields are computed.

Calculations were performed for an RnR Products SB-XC glider; parameters are given in the Appendix. The SB-XC glider is an electrically powered aircraft. Regenerative soaring is allowed in these simulations. The battery pack is assumed to be a 4S1P (4 series, 1 parallel) lithium-polymer battery with total capacity of 4.9 Ah. Pack voltage is 14.8V, resulting in a total capacity of 261 kJ. At a vehicle mass of 10kg the specific energy of the pack is 2748m. For simulations presented here this is reduced to 2500m. Thus for regenerative soaring the total energy expenditure is permitted to reach a minimum of -2500m. Positive values of energy expenditure thus represent energy lost and negative values of energy expenditure represent energy gained from the atmosphere.

3.2.1 Constant Wind

Simple cases of zero wind and horizontal air motion(wind blowing along x axis) are considered. The mesh surface represents the total energy required at that point to reach the goal and the black stream lines on the plane z=0 shows the flight paths to the goal.

From Figure 3.2 shows expected results for the zero wind case. The energy required to reach the goal increases steadily with the distance to the goal. The

stream lines also suggest that flying straight to the goal is the best option for minimizing energy required. The horizontal component of wind "tilts" the cone so that starting points downwind of the goal require more initial total energy to reach the goal than starting points upwind of the goal. The path to the goal also modifies accordingly. This also matches intuition.

Note that uniform Cartesian grids are used, and the effect of the grid can be seen in the solutions. Instead of straight line paths manhattan distances are found to be favored by the trajectory planner. A polar grid will not only smooth cone in the zero wind case but also straight line trajectories to the goal will be observed.

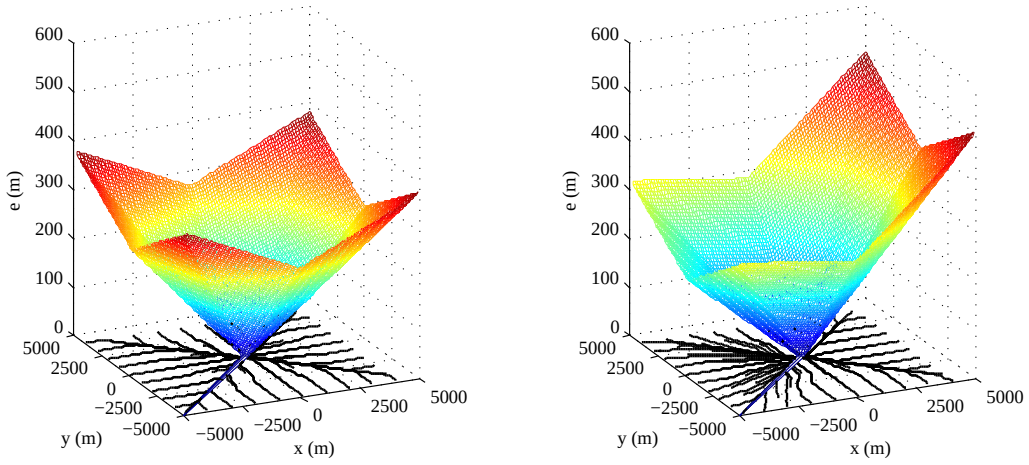

(a) Zero wind

(b) 5 m/s wind in positive x direction

Figure 3.2. Energy maps for a uniform horizontal wind fields..

3.2.2 Horizontal Wind Shear

Wind shear is considered in the second case. Here the horizontal component of wind varies linearly from w_x = 10m/s at y = -5000 to w_x = -10m/s at y = 5000. The energy map as well as trajectories to goal are shown in Figure 3.3. A "twist" in the energy map as expected is noticed. The optimal trajectories are also modified accordingly. The vehicle maximizes exposure to favorable winds and minimizes exposure to unfavorable wind. Starting points in the regions $x > 0$, $y > 0$ and $x < 0$, $y < 0$ show flight paths that remain in the region of high tailwind before turning to approach the goal. For starting points in the regions $x > 0$, $y < 0$ and

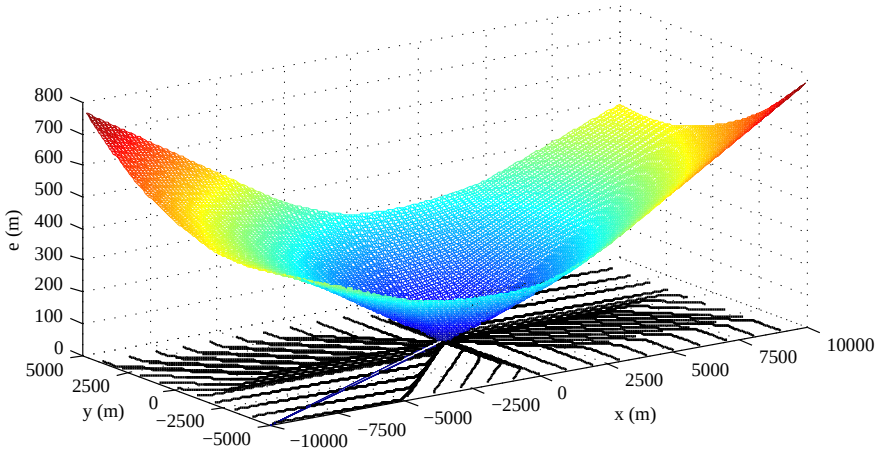

Figure 3.3. Constant wind shear energy map and minimum energy flight paths.

$x < 0$, $y > 0$ the same is true: flight paths begin with motion towards regions of more favorable wind before turning towards the goal.

3.3 Ridge soaring

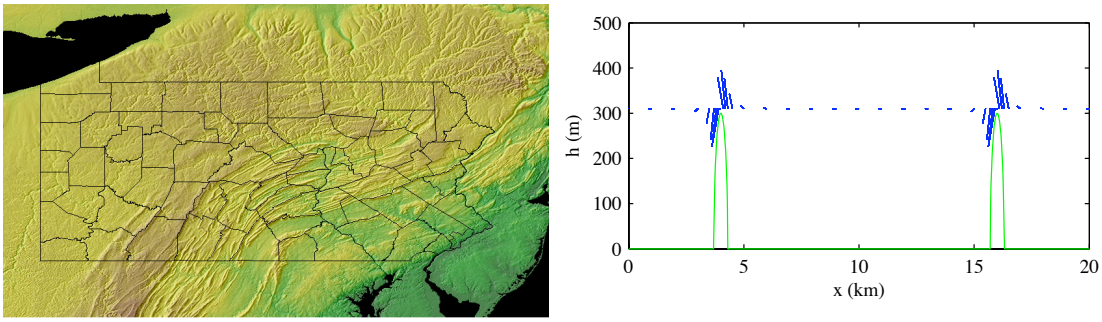

(a) Digital elevation map of Pennsylvania (b) Cross section of parallel ridges and wind field

Figure 3.4. Subfigure (a): Topography of central Pennsylvania showing Appalachian mountains; Subfigure (b): Schematic of ridges and potential flow solution of wind field.

To demonstrate energy maps applied to flight path planning consider flight to a distant goal in terrain representative of the ridges of Appalachian Mountains of Central Pennsylvania.(Figure 3.4). A distance of 12 km separates two parallel ridges.A global coordinate frame is defined with y parallel to the ridges, so that

the ridge centerlines are located at x = 4km and x = 16km. Each ridge is modeled as an infinitely long hemi-cylinder with radius of 300m, to compute the wind field a potential flow method is used. Potential flow cannot model flow separation on the downward side of the ridges. But upward air motion is found on the upwind side. This upwind side is the favorable side where one expects the glider to gain energy. Intuition suggests that the glider will tend to follow the upwind sides of ridges, thus the flow on the downwind sides of ridges is less critical to trajectory planning (except for the times when the vehicle must traverse these non-favorable regions). The results will verify intuition.

The origin is located at (0; 0) and the energy map is computed for an area defined by $0 \leq x \leq 20km$ and $0 \leq y \leq 100km$. Here the wind field is computed at an altitude of 310 m and it is assumed that the wind field does not vary with altitude. The altitude is chosen in such a manner such that it is sufficient to just clear the ridges. Uniform grid spacing is not desirable in terms of practical use. This is because uniform grid spacing may result in inaccurate energy maps, because it is assumed that wind field is constant over an edge or may result in excessive computational requirements (using very fine meshing for example). For this example a non uniform Cartesian grid is used, with finer grid spacing over the ridges, where the wind field changes rapidly over short distances. And wider grid spacing is used between the ridges where the wind is roughly constant. Figure 3.4b shows a vector plot of the computed wind field at the x coordinates of the grid. Spacing varies from a minimum of 100m to a maximum of 1000m. Grid spacing in the y direction is constant at 1000m.

Energy maps for two different cases are considered. In the first case regenerative soaring is not allowed, i.e minimum thrust coefficient of the aircraft is set to zero. Since the aircraft is constraint to move in a plane thus in the regions of upward moving air the speed of the glider increases considerably and no energy is required by the aircraft to travel in these cases.

Figure 3.5 shows the energy map and and paths to fly for a wind field resulting from $w_{x,\infty}$=-5m/s (which results in maximum vertical component of wind of approximately 3m/s along the ridge). The minimum sink rate of SB-XC glider (i.e., minimum rate of altitude loss in still air) is 0.56m/s. Hence the maximum vertical wind speed is enough to gain energy from the ridges. Figure 3.5 shows energy

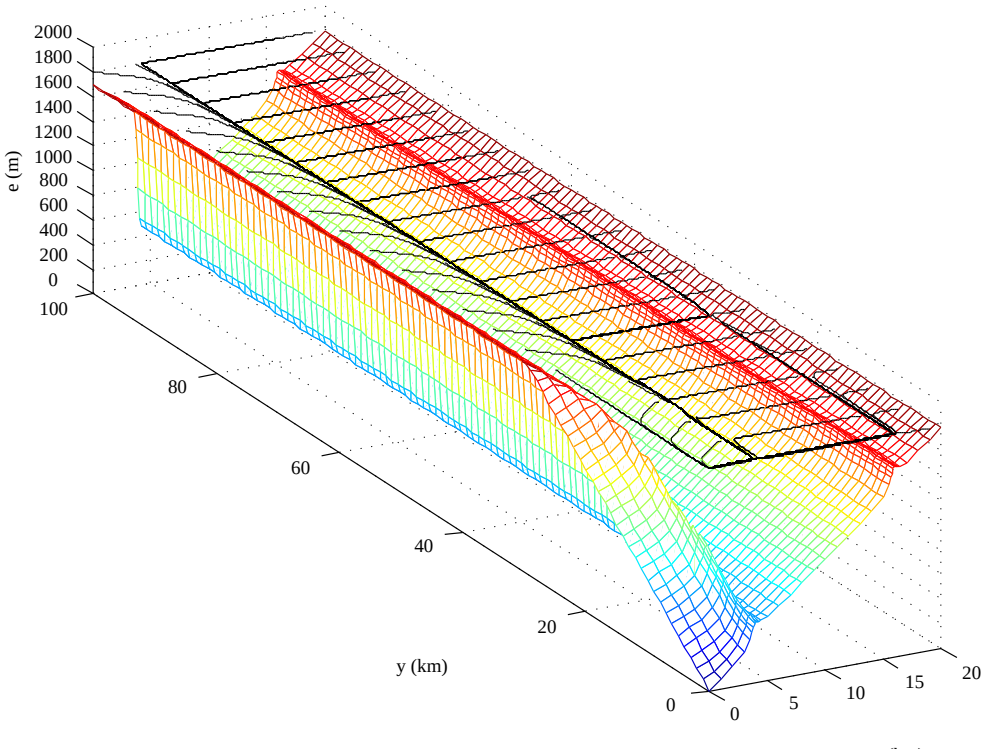

Figure 3.5. Energy Map and paths to the goal in case of Non-Regenerative soaring.

maps regenerative soaring is not allowed. Thus in the regions of upward moving air the energy required to reach the goal remains constant. Constant altitudes of energy in the regions of upside of the mountain ridges are observed. Thus once the aircraft flies into such a region it does not need to expend any energy from its onboard energy source and glide with an elevated speed. There is a small region near the goal where the best path indicated is to directly fly towards the goal. But this region is quite small since it is always advantageous to fly towards the ridge and then proceed towards the goal.

Typically paths follow the upwind side of the ridges. Because regeneration is not permitted (and neither is altitude gain) it is not energetically favorable to fly along the ridge at $x = 16$. It is seen that in the region from $y_0 \geq 60$ and $x_0 \geq 15$ paths instead of following the ridge at $x = 16$ crosses over and comes directly to the near ridge and follows the near ridge before proceeding towards the goal. This happens due to the fact that following any of the ridges are energetically equivalent. Since energy is not gained in the ridges in terms of stored energy which

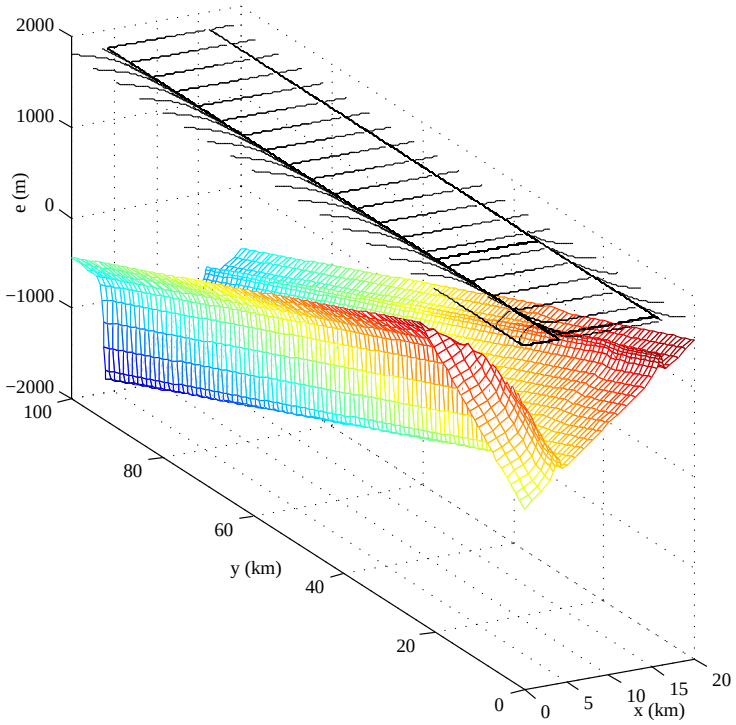

Figure 3.6. Energy Map and paths to the goal in case of Regenerative soaring.

is the driving criteria for the path planning. The maximum energy required from the farthest point to make it to the goal is around 1900 m.

Figure 3.6 shows energy maps where regenerative soaring is allowed. As expected when regenerative soaring is allowed the aircraft can gain a lot of energy from the ridges. Negative energy implies that the aircraft can start with less than fully-charged batteries and still reach the goal. Flight paths are also modified accordingly. One can now see that trajectories starting from region $y_0 \geq 60$ and $x_0 \geq 15$ stick to the far ridge and only make a transition to the other ridge when it is equal in terms of energy. The region of attraction for the far ridge is much wider in this case. Also path constraint dictates how much energy can be gained from the ridges. When regeneration is allowed the maximum energy that can be gained from the atmosphere is almost equal to the total battery capacity of the aircraft. Thus one can gain enough energy starting from anywhere and still reach the goal. Missions involving perpetual endurance can be looked upon as long as the winds keep blowing. Given the constraints on the flight path it is not possible to fully

charge the battery to its maximum value of 2500m in this environment. However, relaxing the progress to goal constraint does allow full charging (discussed in Chapter 4).

3.4 Conclusion

This chapter has defined the Energy Map. The Energy Map approach has been successfully implemented is sample wind cases. The energy map provides energy efficient routes which an airplane should follow to minimize usage of on board energy supply. In addition to providing energetically favorable routes the Energy Map also provide the energy required at each point in the domain to make a flight to the goal. The energy requirement provided by the energy map will immediately answer the question of feasibility of the solution with the aircraft constraints. The important drawback of the energy map is the restriction of always moving towards the goal. The next Chapter demonstrates how much energy can be gained from the ridges if the path constraint of always moving towards the goal is removed. A critical analysis on how much energy is lost by removing the constraint of always moving towards the goal will be made.

Chapter 4

Optimal Paths via Heuristic Search

This chapter describes how heuristic searches can be used for soaring application. The success of heuristic searches is well known for robotic applications. Thus heuristic search procedure will be used for soaring applications.

One can use a variety of informed or heuristic searches to search the nodes of the environment to find the minimum cost path. The A* algorithm is a best-first search algorithm that finds the least costly path from an initial configuration to a final configuration. It uses a cost function or heuristic at each node. For each previous step an exact cost is known while the estimated cost to reach the goal is estimated. One of the requirements of A* is that the cost function must be admissible,i.e., the estimated cost must be less than the actual cost, this produces computationally optimal results.

The A* algorithm is reproduced from [Nilsson,1980], can be summarized as

1. Create a search graph G, consisting only with start node n_0. Put n_0 on a list called OPEN.

2. Create a list called CLOSED that is initially empty

3. If OPEN is empty, exit with failure

4. Select the first node on OPEN, remove it from OPEN, and put in CLOSED. This node is called n.

5. If n is a goal node, exist successfully with the solution obtained by tracing

a path along the pointers from n to n_0 in G. (The pointers define a search tree and are established in step 7.)

6. Expand node n, generating the set, M, of its successors that are not already ancestors of n in G. Install these members of M as successors of $n$in G.

7. Establish a pointer to n from each of the members of M that were not already in G (i.e., not already on either OPEN or CLOSED). Add these members of M to OPEN. For each member,m, of M that was already on OPEN or CLOSED, redirect the pointers of each of its descendants in G so that they point backward along the best paths found so far to these descendants.

8. Reorder the list OPEN in order of increasing $\hat{f}$ values. (Ties among minimum $\hat{f}$ values are resolved in favor of the deepest node in the search tree.)

9. Goto step 3.

A*is *complete*. In the context of trajectory planning *complete* implies that an algorithm is guaranteed to find a solution if one exists. then one can guarantee that no such solution exists.

4.1 Applying A* to Autonomous Soaring

The A* path planning method will be used for long distance trajectory planning to exploit energy from the atmosphere. To the author's knowledge this is the first application of A* for autonomous soaring. As can be seen from the algorithm above the process in which the search process expands is twofold: (1) selecting the next node to visit and (2) and planning the best path through the rest of the graph to arrive at the goal. The cost is a linear combination of two terms: $g(n)$, the cost of best found path so far; and $h(n)$, a heuristic function which is an estimate of cost from node n to the goal. Here h is defined as the straight line distance between the current node and the goal, and thus is an estimate of the time required to reach the goal.

In soaring application the cost function that is used is a weighted linear combination of the two terms:

$$f(n) = \alpha g(n) + (1 - \alpha)h(n) \tag{4.1}$$

The function $g(n)$ is evaluated as the total energy required to reach node n:

$$g(n) = c_{ij} \tag{4.2}$$

where c_{ij} is the cost of the transition ij which reaches node n, and is defined in Section 2.3.

Thus changing the weight α allows changing the cost function to favor energy gain ($\alpha = 1$) or time to goal ($\alpha = 0$). The effect of varying α on the initial energy can be evaluated by computing the energy required to fly the path generated using a particular value of α. Finding the value of α is critical in this context, as both energy expended and time to goal are important parameters governing the utility of a flight path.

4.2 Weighing energy gain vs. distance to goal

The energy map approach described earlier [31] is used as a comparison to evaluate the utility of paths generated using A* approach. The energy map is an upper bound on the minimum energy required to reach the goal in a given wind field. Thus the energy expended in the path when compared with the energy map will give us an intuitive understanding of the critical value of α to choose to successfully use A* for soaring application. The value of α is important tradeoff between energy gained and time to reach the goal. If the value of α is too large the aircraft will will spend too much time looking for energy and not go to the goal quickly enough and if the value of α is too small it wont go easily to the easily exploitable energy sources.

Finding the critical value of α is the key to using A* to soaring problem. In this chapter detailed simulation results are carried out which will enable one to select a particular α which will be best considering the energy that can exploited from the atmosphere also considering the time to reach the goal.

The results obtained from A* will be compared with the energy map approach. It shall become clear that the cost function has an enormous influence on the utility of computed paths.

4.3 Choice of Weight

Simulation of flights through various wind fields are used to find the effective value of α. Two example wind fields are used to examine the effect of the weight α on flight paths: a thermal-like field consisting of two regions of upwards moving air and two regions of downwards moving air and a ridge wind field consisting of two parallel hemi-cylindrical ridges(same environment as the last chapter). For both cases a rectangular Cartesian grid is used to discretize the environment. Allowable transitions can occur to nearest neighbors along the sides and diagonals of the grid.

4.3.1 Thermal-like wind fields

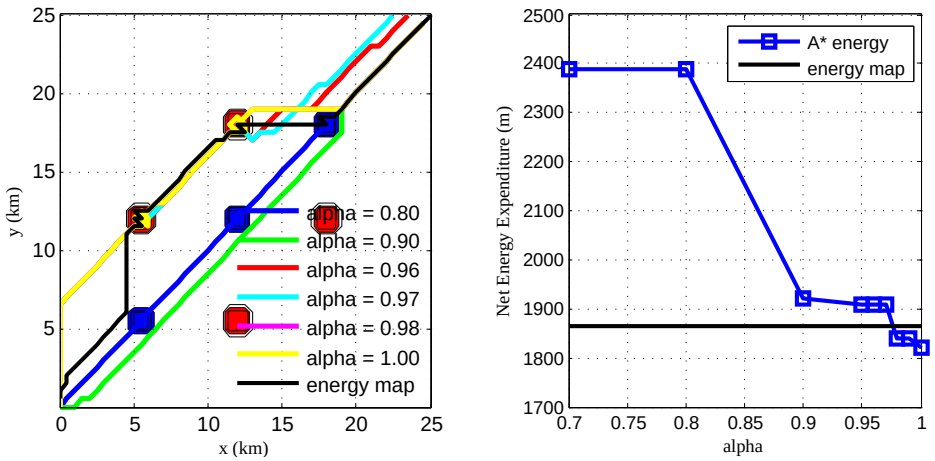

(a) A* paths for thermal-like wind field (b) Variation of required initial energy with α

Figure 4.1. Subfigure (a): A* and energy map paths to the goal; Subfigure (b): Comparison of Energy expended to reach the goal.

Consider a square region of 25kms $\times$ 25kms which is divided in uniform cartesian grid of 50 $\times$ 50 nodes which has different regions of vertical wind (both upwards and downward wind). Upward moving air representative of thermal of

approximate radius of 0.5 Km are located at $(x, y) = (12.5 \text{ km}, 6.25 \text{ km})$, located at $(x, y) = (18.75 \text{ km}, 12.5 \text{ km})$, located at $(x, y) = (6.25 \text{ km}, 12.5 \text{ km})$ and located at $(x, y) = (12.5 \text{ km}, 18.75 \text{ km})$. Similar regions of downward moving air are located at located at $(x, y) = (6.25 \text{ km}, 6.25 \text{ km})$, located at $(x, y) = (12.5 \text{ km}, 12.5 \text{ km})$ and located at $(x, y) = (18.75 \text{ km}, 18.75 \text{ km})$.In Figure 4.1a upward moving air is in the regions shown in red and downward moving air in regions shown in blue. The goal is the origin of the co-ordinate system.

The sample wind field is so chosen as it has both regions where the aircraft can gain energy and lose energy. A "good" path planner should avoid regions where it loses energy but should try to fly in proximity of those regions where it can gain energy. This example also shows the effect of discretization on the final solution.

Figure 4.1a shows paths to goal from a distant point of $(x, y) = (25km, 25km)$. As the weight factor α is varied between zero and one, the path planned for the UAV shows clear changes. When α equals zero there is no weight on the energy available from the atmosphere and the cost function is driven by only the distance to goal. In this case all paths with $\alpha < 0.8$ behave similarly, and the optimal path is straight to the goal, thus the aircraft flies straight through the energetically unfavorable regions of downwards moving air. The blue path in Figure 4.1(a) shows that this is indeed followed. When $\alpha = 0.9$ the path avoids the regions of downwards moving air (green path) but does not divert further to exploit the energy in the other rising pockets.

As the value of α is increased further ($\alpha > 0.96$) paths begin to exploit upwards moving air. More time is spent in the region of upwards moving air as more emphasis is placed on energy gain. When $\alpha = 1$ time to goal is irrelevant, and the flight path traverses every node where energy gain is possible. Note that the path still does not crosses to other nodes where there are unexplored regions of upward moving air. This is because the thermals are too small to make it worth the energy gain that the aircraft will expend along the path to reach the thermals. The path in black shows the energy-map computed path [31].

For each value of α the energy expended along the path is calculated. As seen from Figure 4.1b the energy expended for $\alpha = 1$ is much lower compared to the other values. Energy expended for values of $\alpha \leq 0.8$ is high as the paths goes straight through the regions of downward moving air. Energy expended is

considerably reduced for $\alpha \geq 0.9$ as the aircraft starts avoiding the unfavorable wind. But the real jump in the energy expended is found at $\alpha = 0.96$. For values of $\alpha > 0.96$ the energy expended along the path is lower than that expended if followed the energy map path.

Comparing the energy expended for each path shows the influence of the distance:energy weight on the computed paths. Further, comparison with the energy map path shows that for $0.96 < \alpha < 0.97$ the required initial energies are roughly equal. Higher weights on energy reduce required initial energy but the cost is significantly longer paths to goal. Similar results were found for planning scenarios using ridge-like wind fields.

4.3.2 Ridge Soaring

Terrain representative of the Appalachian Mountains (the same as used earlier for the Energy Map approach) is used to analyze the A* approach. The results are compared to energy map and energy map is used to find the right cost function as well. Recall that the energy map is the upper bound on the minimum energy required to the goal. Thus energy map will be a good mode of comparison to find the correct cost function.

Simulation results were carried out with $w_{x,\infty} = -5$m/s (which results in maximum vertical component of wind of approximately 3.0 m/s along the ridge). The wind blows from right to left. Thus there is upward moving air (which permits energy extraction) on the right side (positive x) of the ridges. Flight paths were computed for four different starting positions: $(x,\ y) = (20\text{km},\ 100\text{km})$, $(x,\ y) = (20\text{km},\ 50\text{km})$, $(x,\ y) = (20\text{km},\ 20\text{km})$, and finally $(x,\ y) = (10\text{km},\ 70\text{km})$. Flight paths were generated for each starting position for varying values of α and results are compared with flight path computed using the energy map. Here results from only one of the starting points, namely $(x,\ y) = (20\text{km},\ 100\text{km})$ are shown. Starting points from the other regions also produced similar results. The results for other starting points are given in Appendix B.

From Equation 4.1 it is evident that for $\alpha = 0$ the energy required is not included in the total cost function. Figure 4.2a shows the path to the goal from a distant point of x=20 km and y=100 km. As α is varied from 0 to 1 flight paths

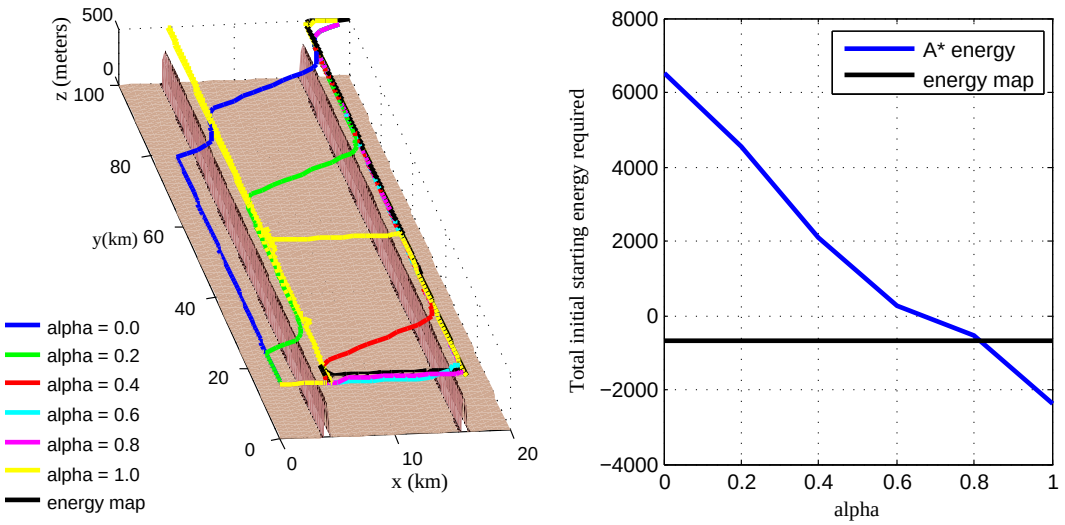

(a) Comparison of A* paths and Energy Map path

(b) Initial Starting energy for varying α and energy map

Figure 4.2. Left: Different paths to the goal starting from x=20 km and y=100 km; Right: Comparison of the initial starting energy for x=20 km and y=100 km

goes more in the regions of upward moving air. For α=0 the path goes straight towards the goal. Note the effect of grid on the path. Instead of moving straight towards the goal the vehicle opts to proceed towards the diagonal first. As the value of α keeps on increasing the flight paths are seen to wander near regions of the upwind where it can gain energy. The energy map path is also shown in the same figure. For $\alpha = 0.8$ almost similar path is seen than that of energy map. The energy map path always moves towards the goal. It leaves the first ridge and moves over to the second ridge in between as those two will have same energy gains and are effectively equivalent paths. The path for $\alpha = 1$ is interesting. Flight paths are seen to zigzag in the first ridge and then when all the nodes are exhausted the path crosses over to the next ridge. Upon reaching the next ridge the aircraft continues to gain energy moving to and fro in the upwind side of the ridge and eventually reaches the goal.

Figure 4.2b shows the expended energy for different values of α. Results match the intuition that as the importance of energy gain is increased, the net expended energy is reduced. Because the starting point is at the extremum of the task area the A* path (which would otherwise allow motion away from the goal) is equivalent

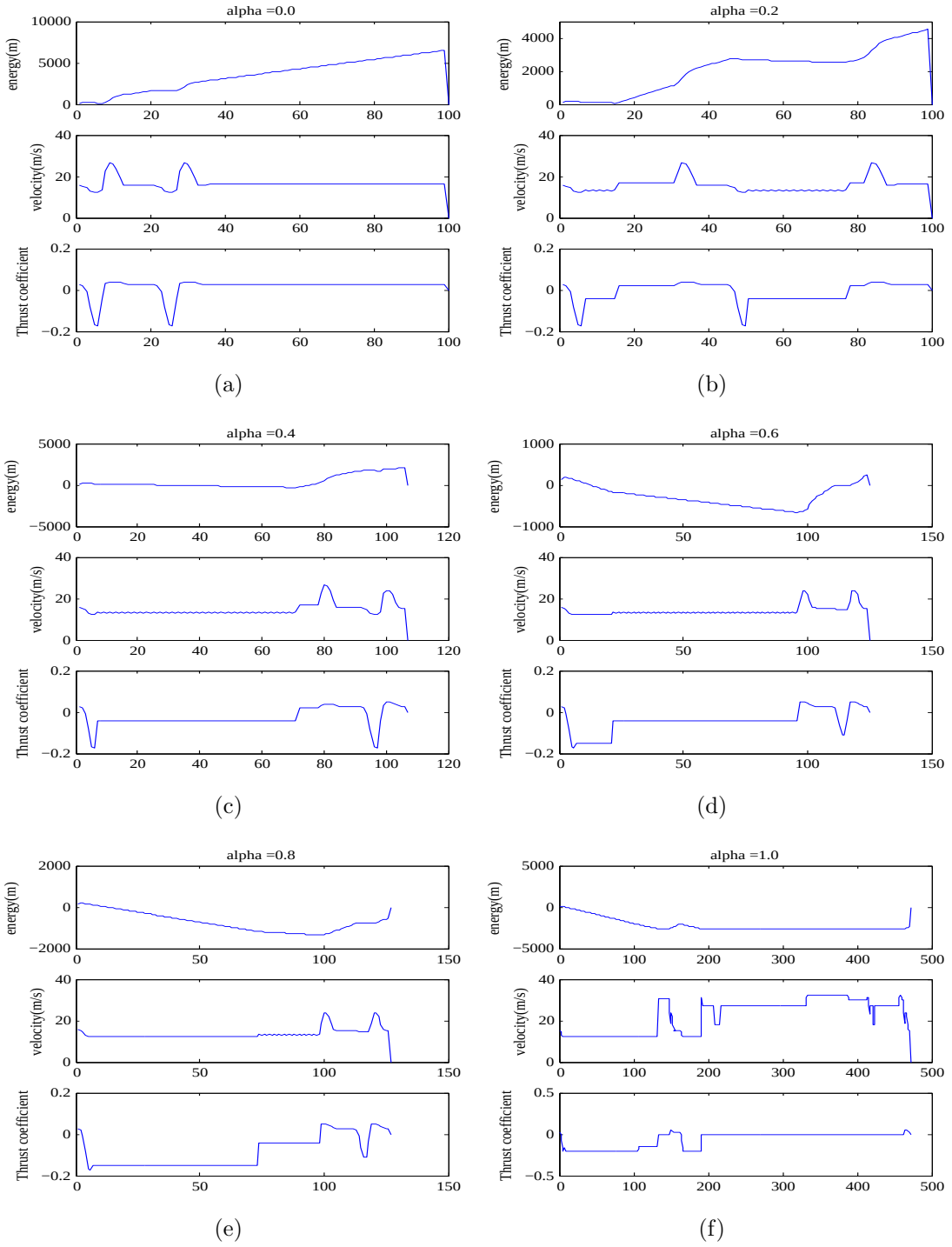

Figure 4.3. Energy, Velocity and Thrust Coefficient along the paths for different values of α

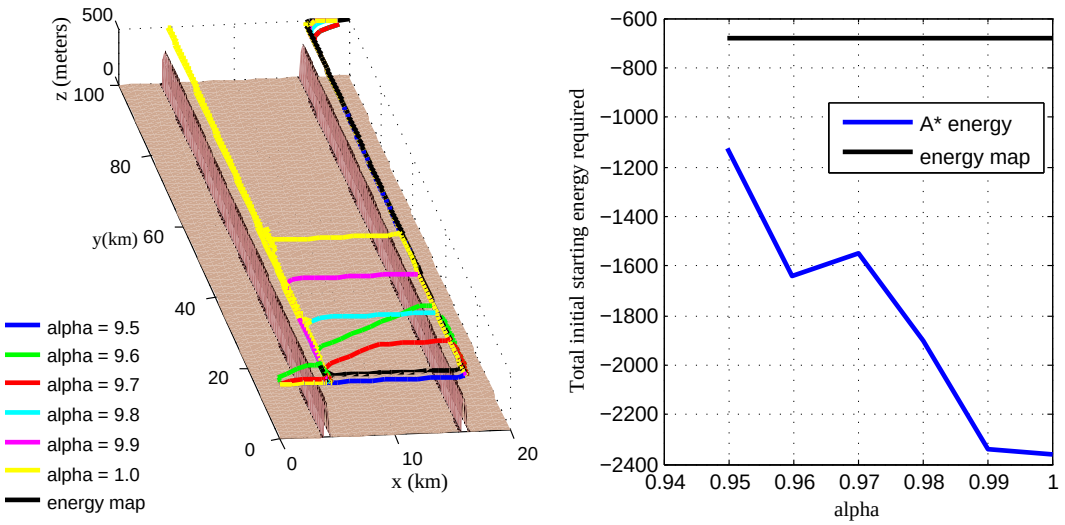

(a) Comparison of A* paths and Energy Map path

(b) Initial Starting energy for varying α and energy map

Figure 4.4. Left: Different paths to the goal starting from x=20 km and y=100 km; Right: Comparison of the initial starting energy for x=20 km and y=100 km

to the energy map path (which does not).

Figure 4.3 shows the value of energy, velocity and thrust coefficient along the path for different values of alpha. For $\alpha = 0$ as seen from Figure 4.3a the energy required increases steadily. Also note that with a battery capacity of 2500m a flight path straight to the goal is not feasible, thus energy gain from the atmosphere (i.e. soaring flight) is required to reach the goal. There are two places where the energy dips a little bit. These are the regions where the path crosses the ridges. The velocity profile shows an increase in velocity while moving through the downward air in the lee ward side of the mountains, while velocity decreases and thrust coefficient touches negative as the vehicle passes through the regions of upward moving air. For the other cases of α one can see such values of velocity and thrust coffering as the aircraft crosses the ridges. As the value of α increases total energy required decreases. It can be seen from the velocity profiles that the aircraft spends very little time in the leeward side of the mountain where it loses energy. Velocity in this cases hits the peaks. For $\alpha = 1$ the energy dips very quickly and hits -2500m. This is the point where regenerative soaring is stopped and minimum thrust co-efficient is set to be zero because the batteries are fully charged. Thus

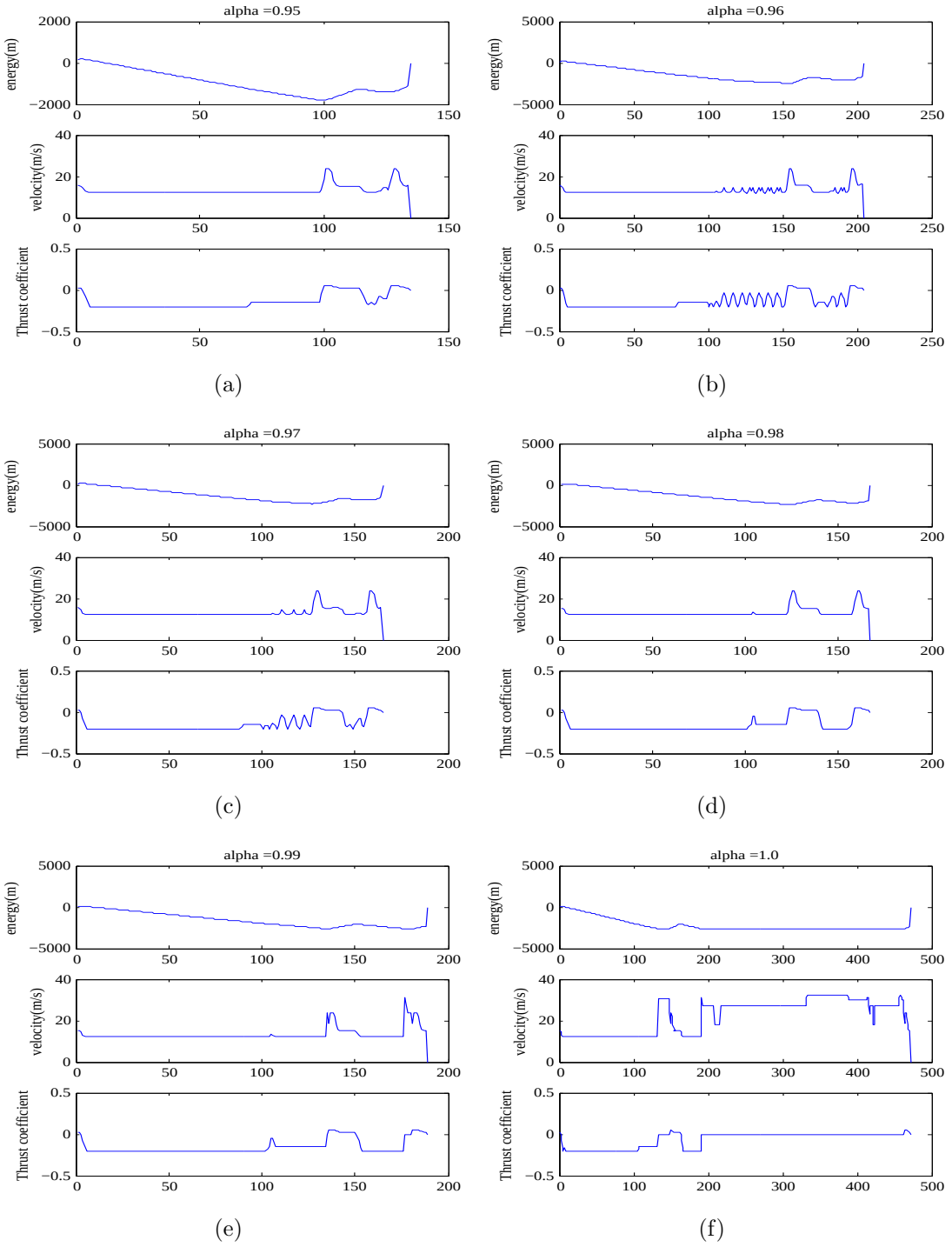

Figure 4.5. Energy, Velocity and Thrust Coefficient along the paths for different values of α

velocity shoots up and thrust remains zero. It is at this point the aircraft decides to leave the first ridge. While crossing over to the other ridge the aircraft has to again expend energy and one can see drop in velocity and increase in thrust coefficient. After reaching the second ridge again the vehicle gains energy and hits -2500 m of energy and thrust coefficient remains zero for the next rest of the path and also the velocity becomes high.

Thus in these cases one can see a significant drop in energy expended as α is varied from 0 to 1. Increasing alpha reduces the starting energy required but the time to reach the goal also increases dramatically (as indicated by the number of nodes traversed during the flight: 500 nodes are traversed for $\alpha = 1$ while less than 100 nodes are traversed for $\alpha = 0$).(Note the difference in scales of horizontal axes).

Thus to find an effective value of α results with higher values of alpha were analyzed.

Figure 4.4a shows the paths to the goal as α is varied between 0.95 to 1.0. Close observation of the paths reveal that there is a certain value of alpha which shows a finite jump in the trajectory. For $\alpha = 0.96$ the path for the first time goes to and fro through the ridge and then crosses when the distance function takes over. From Figure 4.4b also one can see that there is a sharp decrease in energy required to reach the goal as α is increased from 0.95 to 0.96. If alpha is increased further there is little improvement in terms of energy required. For $\alpha = 1$ the energy reaches the maximum value of maximum allowable charging limit of the batteries.

Similar flight paths are generated four different starting positions: $(x,\ y) = (20\text{km},\ 100\text{km})$, $(x,\ y) = (20\text{km},\ 50\text{km})$, $(x,\ y) = (20\text{km},\ 20\text{km})$, and finally $(x,\ y) = (10\text{km},\ 70\text{km})$. After analyzing the data obtained from all the starting positions the critical value of α for which energy gain can be maximized without redundant paths is found to be $\hat{\alpha} = 0.96$. The results are give in Appendix B.

From Figure 4.5 shows the energy, velocity and thrust coefficient for the different values of α. $\alpha = 0.96$ shows saw tooth nature of the velocity and thrust coefficient. This happens due to zig-zag flying of the aircraft through the upwind side. Thus $\alpha = 0.96$ seems to be the transition value of alpha where there is correct correlation between energy gained and distance left to travel. Higher values

of alpha leads to redundant paths which increase the time to reach the goal unnecessarily. It is interesting to note that results for $\alpha = 0.96$ show longer paths to goal, and greater energy gain, than for $\alpha = 0.97$ through $\alpha = 0.99$. This runs counter to intuition, and will be examined further in future works.

4.4 Conclusion

This chapter has shown that the A* approach which weights energy and time to goal is able to plan "energy efficient" trajectories for soaring applications. By changing the relative weight of energy cost vs. distance to goal qualitative statements about flight paths can be made, but the flight paths show a strong jump once $\alpha \geq 0.96$. Once value of energy weight causes the flight path to divert from the goal in favor of gaining energy, flight paths will divert as far as the task area allows, with no means of heading to the goal once "sufficient" energy has been gained. This suggested that the upper limit on "useful" values of energy weight is roughly 0.96. Similar results are seen from other starting point in the ridge. The results are given in Appendix B. These simulation results are now applied to see the performance of A* in a real environment.

Chapter 5

Flight in a Realistic Wind Field

The previous chapters have shown two methods of planning for autonomous soaring namely the *The Energy Map* and A* methods. Most useful cost function of A* has been identified through simulation results. In this chapter real wind field data is used to evaluate the performance of the two methods. A critical comparison will be made about the energy map approach for path panning.

5.1 Realistic wind Field

A sample wind field was obtained from the Department of Meteorology at Penn State (courtesy George S. Young, Brian J. Gaudet, Nelson L. Seaman and David R. Stauffer [32]). The wind field represents the evolution of mountain wave over Central Pennsylvania from 0000h UTC to 1200h UTC on October 7, 2007, and was computed using the Weather Research and Forecasting Advanced Research WRF (WRF-ARW) version 2.2.

A visualization of this wind field showing regions where energy can be harvested (i.e. where the vertical component of the wind speed is greater than the minimum sink rate of the aircraft) is shown in Figure 5.1. Blue isosurfaces bound energy harvesting regions, with subfigures (a) through (e) showing the time evolution of the wind field. Note the significant spatial as well as temporal variation of the wind field, leading to a particularly challenging planning problem. Clearly a "good" path planning algorithm will find trajectories that fly through these regions while avoiding regions of downwards moving air.

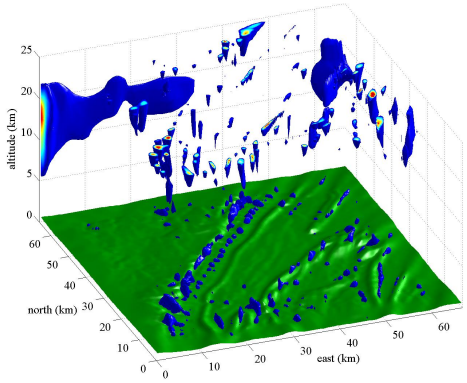

(a) t=0000h UTC

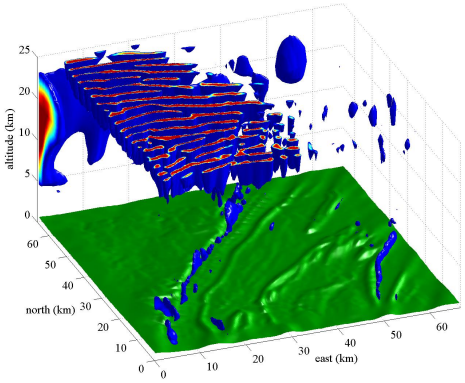

(b) t=0330h UTC

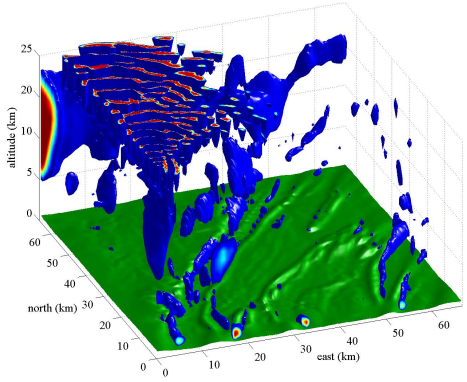

(c) t=0700h UTC

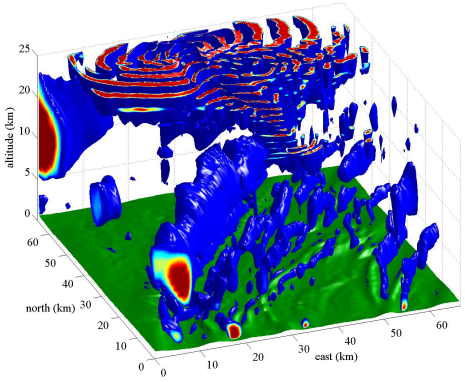

(d) t=0930h UTC

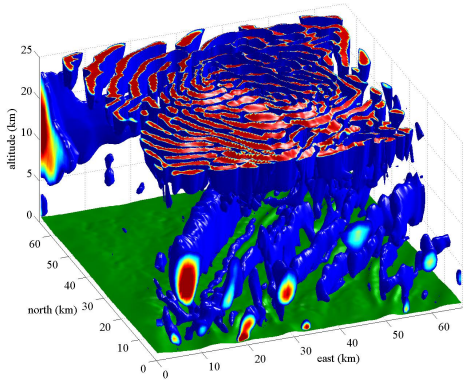

(e) t=1200h UTC

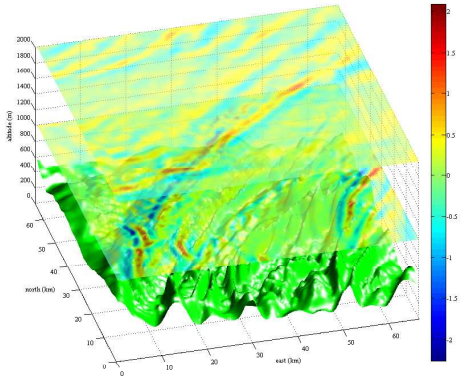

(f) slice at t=0700h UTC

Figure 5.1. Visualization of wind field data for a realistic wind field.

As before it shall be assumed that constant altitude flight is required, either to ensure separation from other aircraft or to satisfy mission parameters such as sensor coverage. Further, the mission at hand is flight towards a goal, and it is assumed that in this context the aircraft flies quickly compared with the rate of change of the wind field. Two simplifications to the planning problem can then be made: first, only the winds at the desired cruise altitude need to be modeled; second, temporal variations in the wind field can be ignored. Trajectories for flights at two altitudes (1000m MSL and 2000m MSL) will be computed and compared using the energy map and the heuristic search. A contour plot showing the vertical component of wind field at 1000m MSL and 2000m MSL (at 0700UTC) is shown in Figure 5.1(f).

5.2 Energy Map

In this example a uniform cartesian grid with node spacing 444m is used. This node spacing is derived from the spacing of the wind field data. The goal is located at (40km,45km). The Energy map is calculated to reach the goal from all points in the environment. Separate energy maps are calculated for two different altitudes. Figure 5.2a shows the energy map in the domain and paths to reach the goal over the energy map. From the figure it is evident that the energy to reach the goal is affected by the given wind field data. The energy to reach the goal from the regions where there is updraft is very low as shown by the blue regions. Figure 5.2b reveals the presence of updrafts in the low energy regions shown by the energy maps. Energy to reach the goal from other parts in the environment is significantly higher. As seen from the paths to reach the goal the planner successfully finds its way to the goal following regions of low energy required, or regions of updrafts as shown in Figure 5.2b.

Similar calculations are made for wind field at an altitude of 2000m. Figure 5.3a and Figure 5.3b shows the energy map and path to goal over the wind field. Spatial wind variation results in slight modification of energy efficient paths than for lower altitude. But a similarities in path in both the altitudes can be attributed to the terrain influence on the wind field data.

Thus in this region these routes can be identified as the most energy efficient

routes and aircrafts trying to reach the goal should follow these routes to minimize onboard energy expenditure. The energy map paths successfully follow the energetically favorable regions and also avoids regions of downward moving air.

The energy map also provides an insight on what stored energy will be required by an aircraft to reach the goal. Thus feasibility of use of certain UAVs will depend on their payload capacity in this kind of wind fields.

As a comparison flight paths were generated using the A* algorithm in similar wind conditions.

5.3 A* paths

Paths from eight starting points distributed around the domain to a goal located near (40,45) are shown in Figure 5.4. For all paths the weight function was set to the value $\alpha_{critical} = 0.96$ found using the simplified wind fields.

Figure 5.4 shows A* paths to goal from eight different starting locations to the goal for two altitudes. Both the figures show similar trends given the similar wind fields. In Figure 5.4(a) paths originating in the north and northwest corners merge in the middle to regions of favorable wind. Similarly two paths which originate in the south and south-east corner of the map cross a narrow region of downwards moving air and then joins before moving on to the goal.

Figure 5.4(b) also shows similar "corridors" in the results. Two paths which originate in the south and south west corner merge in the region of strong upward moving air. Paths originating from the south west also merge in this path near just before the goal. Path originating from the north-west faithfully follows regions of relatively upward moving air while avoiding any downward moving air. Finally paths originating from north and northeast joins the other two just before reaching the goal. Thus routes for the given wind field data that vehicles should follow to optimize their energy requirement and time to reach the goal are identified. Qualitatively the paths follow regions of upwards moving air, but there are some cases where energetically more favorable paths would seem to exist. For example the path starting from south west corner in Figure 5.4(a) should have followed the more favorable wind and merged with the path originating from the bottom middle.

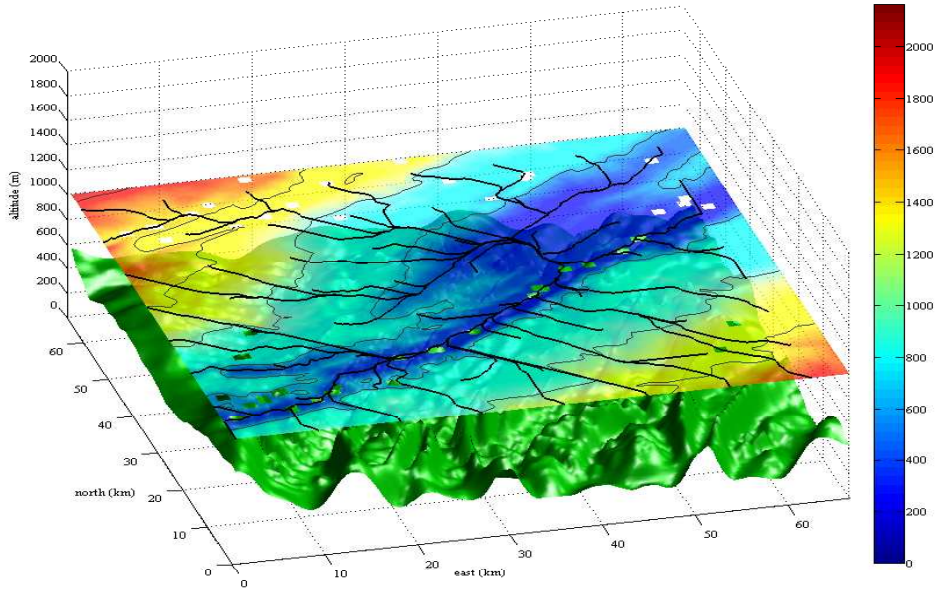

(a) Energy Map at 0700 UTC at altitude of 1km

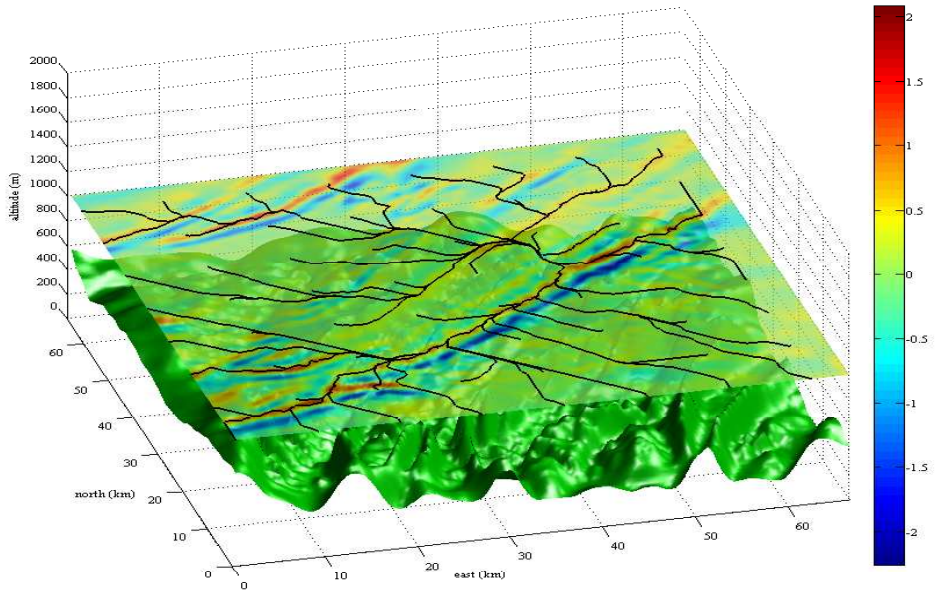

(b) Energy Map Paths to reach the goal over wind field at 0700 UTC at altitude of 1km

Figure 5.2. Energy Map, and Energy Map Paths to reach the goal over wind field at 0700 UTC at 1000 MSL

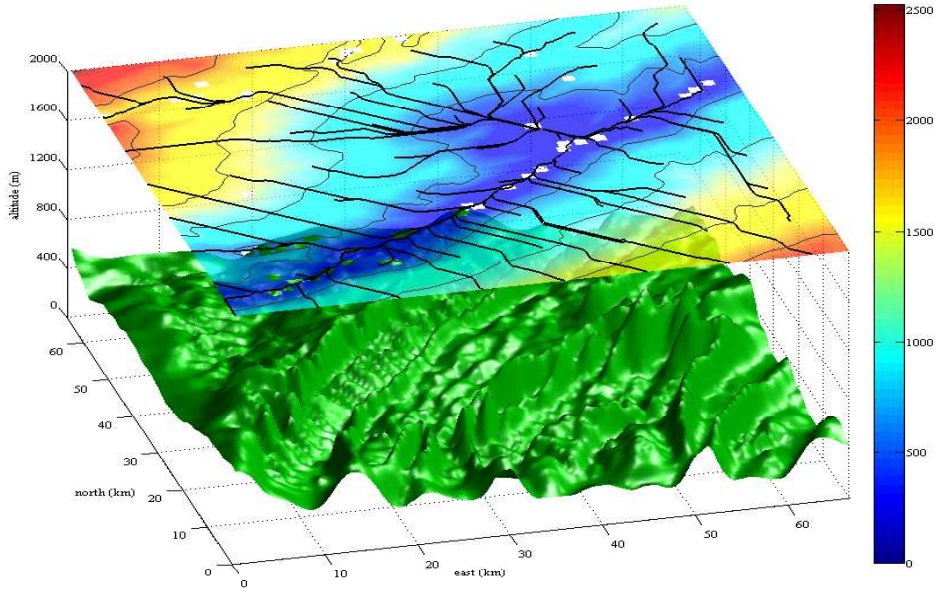

(a) Energy Map at 0700 UTC at altitude of 2km

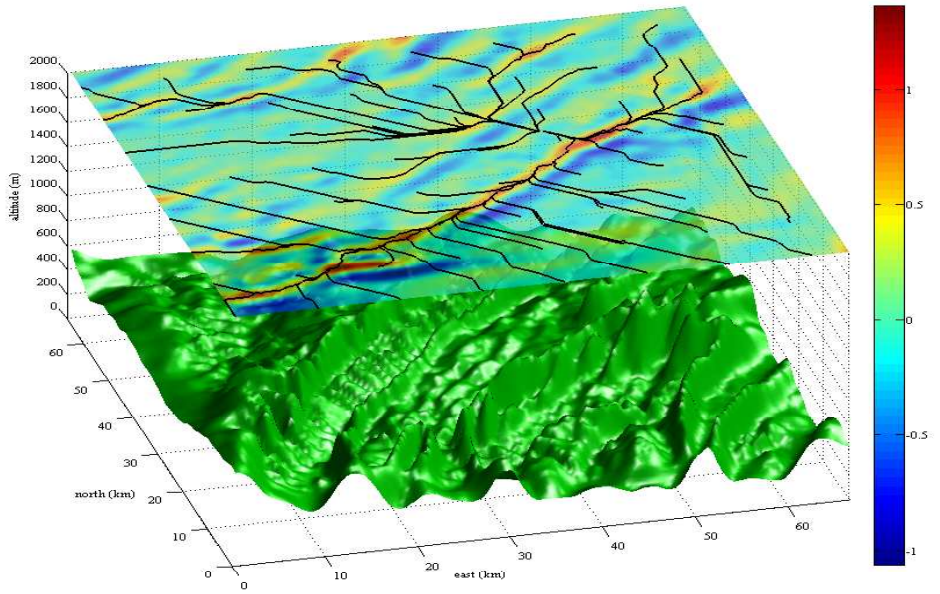

(b) Energy Map Paths to reach the goal over wind field at 0700 UTC at altitude of 2km

Figure 5.3. Energy Map, and Energy Map Paths to reach the goal over wind field at 0700 UTC at 2000 MSL

Thus a comparison with energy map reveal similar paths predicted by both the methods. Even A* could not find any practical energy efficient route other than what predicted by the energy map. Of course with a more weighage on the expenditure of energy term more energy efficient routes could have been exploited but such paths may not be useful for any practical application. Thus both methods can be used successfully for wind routing problems in given wind fields.

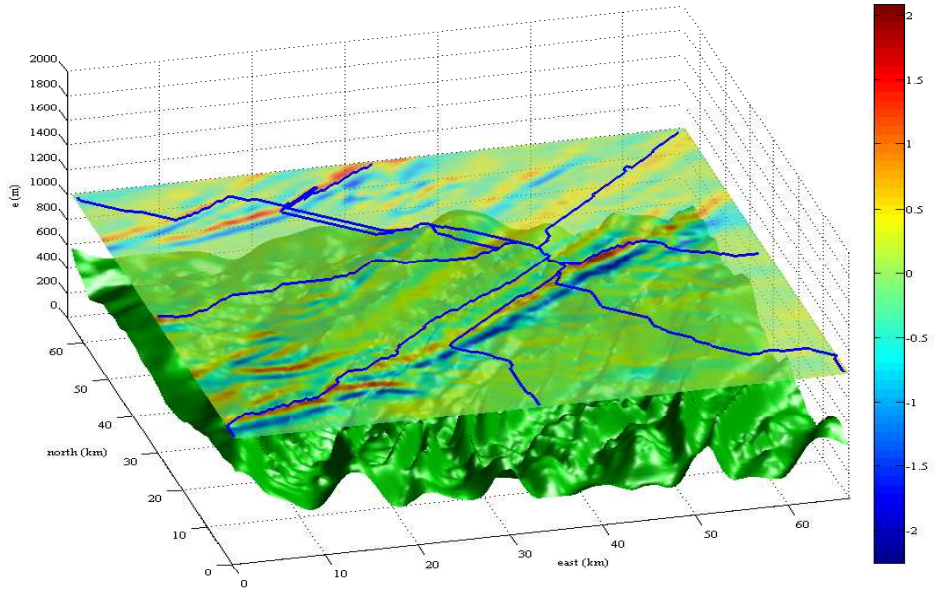

(a) A* Paths to reach the goal over wind field at 0700 UTC at altitude of 1km

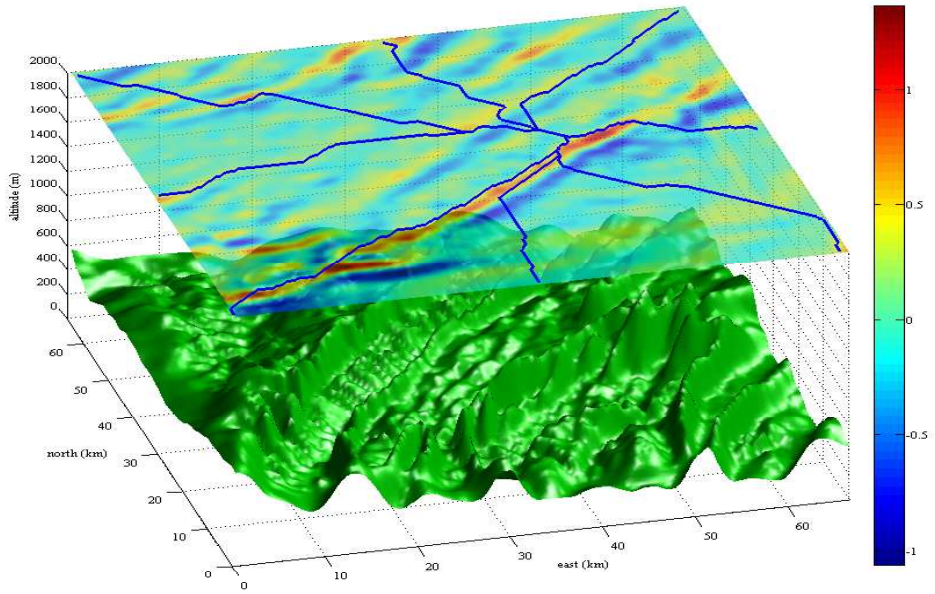

(b) A* Paths to reach the goal over wind field at 0700 UTC at altitude of 2km

Figure 5.4. A* Paths to reach the goal over wind field at 0700 UTC at two different altitudes

Chapter 6

Conclusion

This thesis has presented how graph based planning methods can be utilized for soaring application. The continuous domain is first discretized by waypoints or nodes. Then a mathematical framework to maximize range flight or minimizing energy lost over a segment has been described. The energy expended over a segment is used as the cost function for transition between two nodes. The speed to fly over an edge in the graph is computed by minimizing the energy expenditure for that segment, including the effects of three dimensional wind. Regeneration (conversion of potential or kinetic energy to stored electrical energy using a windmilling propeller or ram air turbine) is included, thus the net required energy for flying a path to the goal can be computed. The optimal flight path planning has been done by two methods

- Energy Map
- A*

In the energy map approach the energy-optimal path is computed using wavefront expansion from the goal, keeping track of the cumulative minimum total energy required to reach the goal. This energy map can immediately indicate whether a feasible path to the goal exists for a particular starting way point and initial stored energy of an aircraft.Paths generated using the energy map can be used as an immediate, possibly sub-optimal solution, or the energy map derived path can be used as an initial guess for further trajectory optimization. The energy

expended along the path can also be used as part of a cost function which may include other considerations (e.g. time to reach the goal), and can be used with generic path planners.

One of the greatest assets of this method is the decoupling of the generation of nodes and the calculation of energy. Thus the computation of path planning is done in two stages. This independent calculation of energy grid makes it useful to use in different grids. The other useful aspect of this method is that this really speeds up the time to compute the energy map and thus path planning. Thus this method may be implemented for real time applications. The challenge is to implement the method in case of changing environments. The time to compute the energy map suggest that it may be possible to use it for real time applications in case of changing environments. Our future endeavors will be directed in these directions.

The energy map is computed using a constraint that all transitions must be towards the goal. This constraint means that lower energy paths which first proceed away from the goal may exist, thus the energy map defines an upper bound on the minimum energy required to reach the goal.

The constraint of always moving towards the goal was not imposed in the second case, where A* algorithm is used. Transitions are allowed to all the neighboring nodes from the start position. The A* algorithm uses a weighted sum of required energy and distance to goal as the cost function. A critical parameter is the value of weight which balances energy expenditure versus progress to goal: improper choice can result in either energetically unfavorable paths or in paths which meander without sufficient progress to goal.

Scenarios involving simplified wind fields (a thermal-like wind field and a ridge wind field computed using potential flow) were used to find a good value of the weighting factor. For the scenarios examined here a sharp jump occurs in planned trajectories once the weight parameter reaches a critical value. After this jump flight paths follow the route of maximum energy gain without further refinement for reducing time to goal. This suggests that there is a maximum practical value of weight beyond which flight paths, while feasible, are not particularly useful.

Finally this thesis applied the two methods of flight path planning in a realistic wind field computed using a high-fidelity forecasting tool. Both the methods were

successful in identifying energy efficient routes in the wind field. The energy maps computed for the wind field gave an insight on the internal energy required for UAVs to be used in this wind field. The effect of terrain was clearly visible for the flight paths calculated.

6.1 Recommendation for Future Works

The two methods discussed in the thesis have been successful in identifying energy efficient routes individually, and both the methods have given feasibility of paths planned for UAVs. It will be an interesting work to combine the two ideas. The Energy map gives us an upper bound on the minimum energy that the vehicle should possess to reach the destination. Thus if a vehicle has on board stored energy less than that indicated by the energy map it in principle cannot reach the goal flying always towards the goal. Here A* may be used to identify energetically favorable pockets in the domain and gain sufficient energy in order that there is enough available on-board energy to reach the goal.

The cost function included in A* approach included remaining distance to reach the goal. Including time to reach the goal instead may improve the results. A dual of energy efficient routes namely time efficient routes may also show some interesting trends. A combination of distance and time may also be looked upon for energy harvesting.

Another most important improvement that needs to be incorporated in the planner is the ability to handle time varying wind fields. Also since atmosphere is not predictable the model should be able to handle uncertainties.

Extending work to permit full three dimensional flight paths will be a significant computational challenge (likely requiring an enormous increase in graph size) but will allow significantly more sophisticated paths.

Appendix A

Vehicle Properties

Note that a fourth order polynomial is used to relate C_D to C_L: this provided a better fit to the computed data over the full speed range.

Table A.1. Parameters for SB-XC glider.

variable	value	description
m	10 kg	mass
S	1 m^2	wing area
$f(C_L)$	$0.1723C_L^4 - 0.3161C_L^3 + 0.2397C_L^2$ $-0.0624C_L + 0.0194$	
$v_{a,min}$	12 m/s	
$v_{a,max}$	35 m/s	

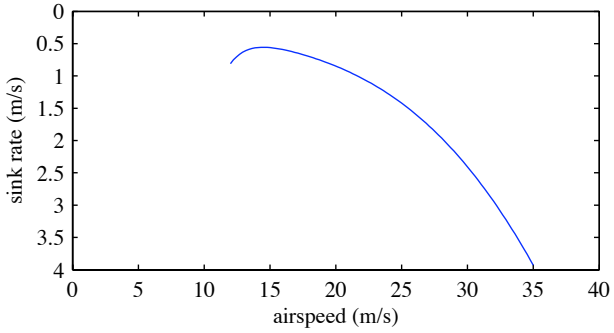

Figure A.1. Sink rate vs. airspeed for the SB-XC. Minimum sink is approximately 0.56 m/s and occurs at approximately 14.6 m/s.

Appendix B

Ridge Soaring Different Starting points

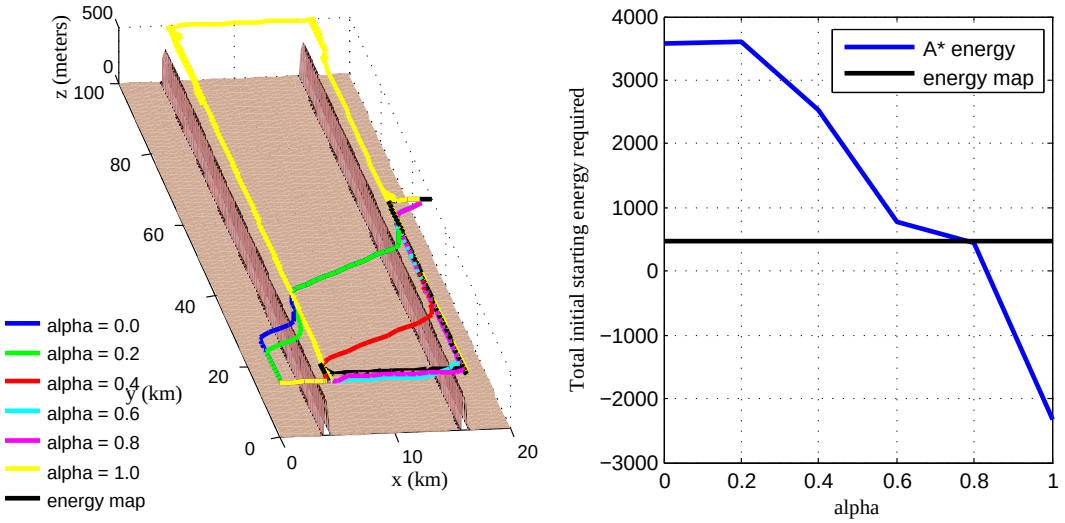

(a) Comparison of A* paths and Energy Map path

(b) Initial Starting energy for varying α and energy map

Figure B.1. Left: Different paths to the goal starting from x=20 km and y=50 km; Right: Comparison of the initial starting energy for x=20 km and y=50 km

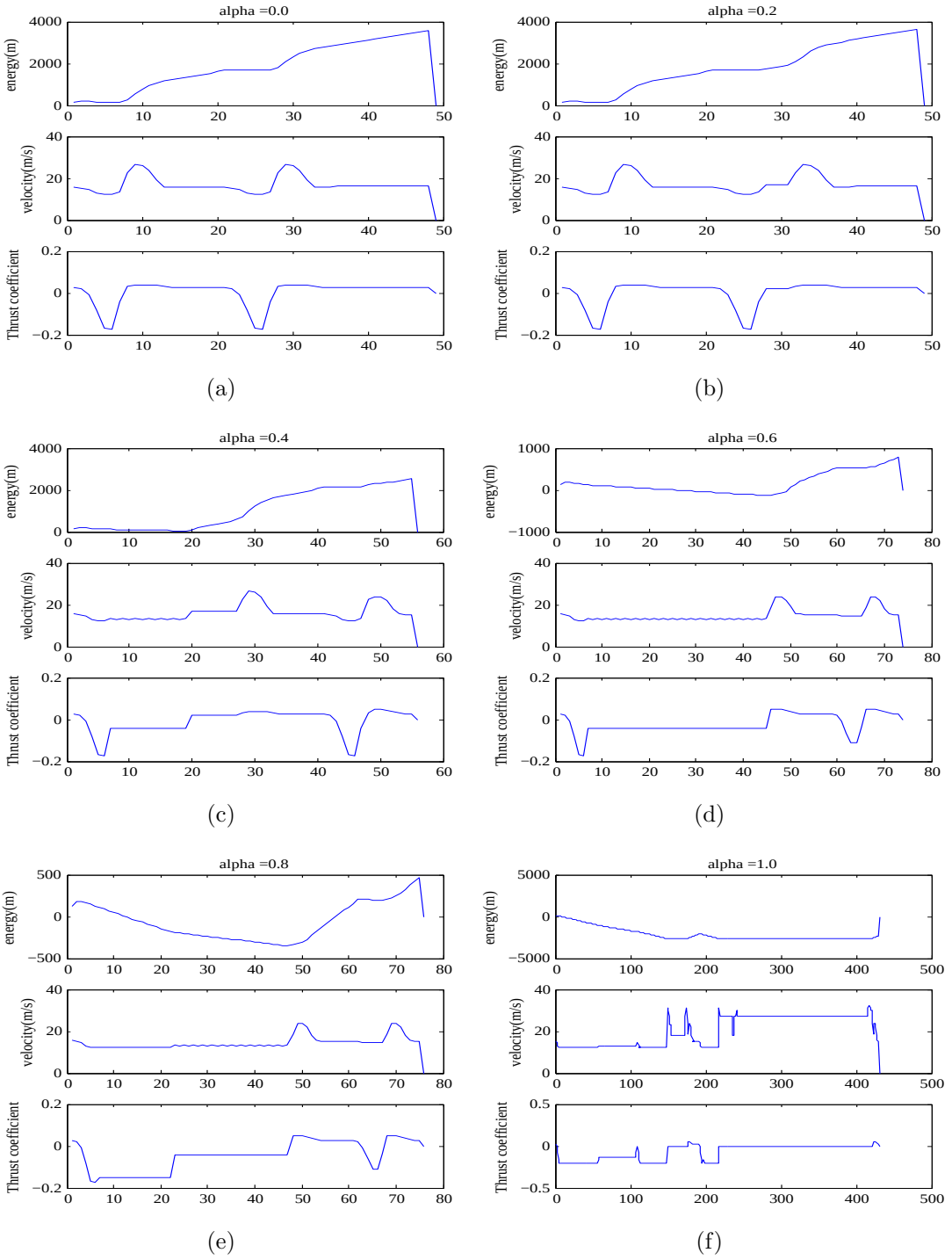

Figure B.2. Energy, Velocity and Thrust Coefficient along the paths for different values of α

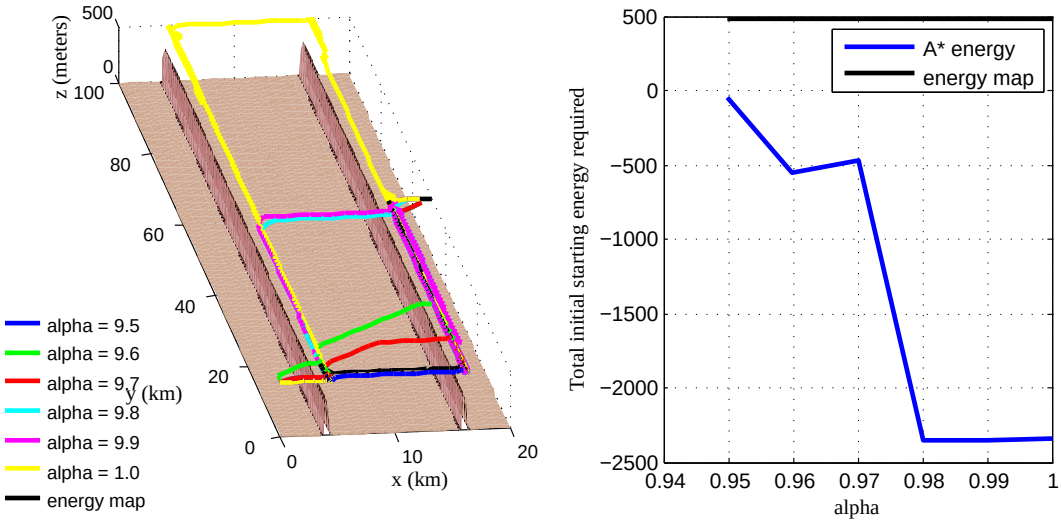

(a) Comparison of A* paths and Energy Map path

(b) Initial Starting energy for varying α and energy map

Figure B.3. Left: Different paths to the goal starting from x=20 km and y=50 km; Right: Comparison of the initial starting energy for x=20 km and y=50 km

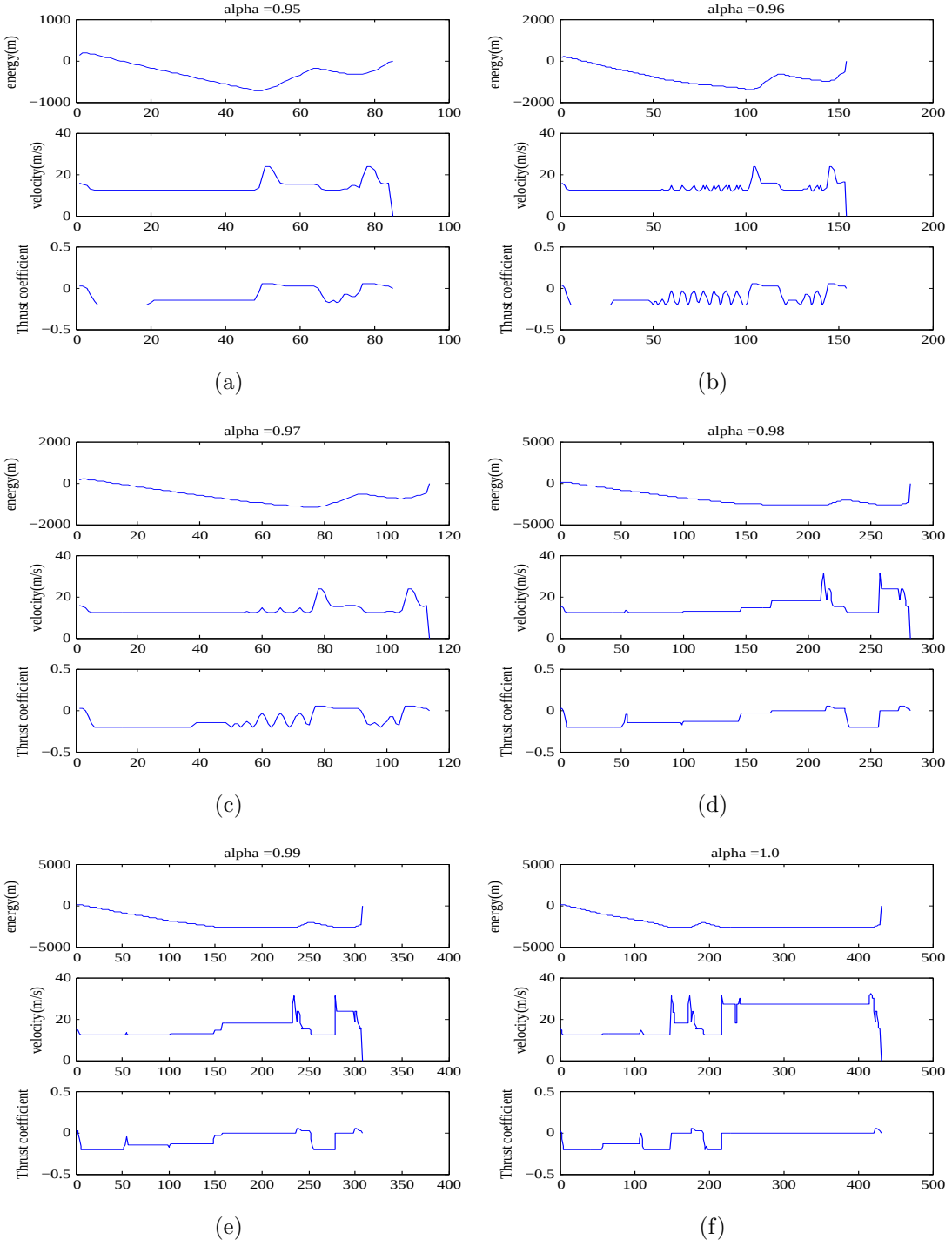

Figure B.4. Energy, Velocity and Thrust Coefficient along the paths for different values of α

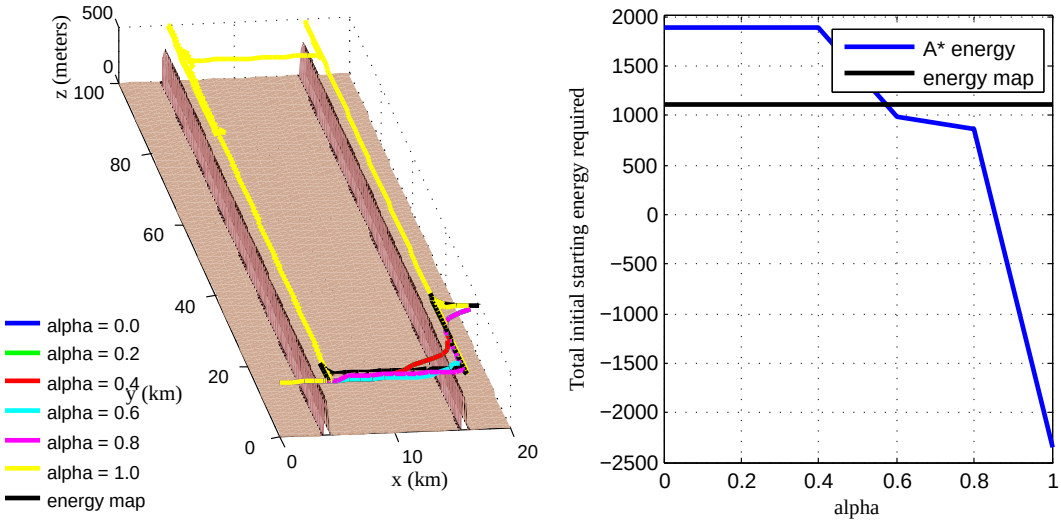

(a) Comparison of A* paths and Energy Map path

(b) Initial Starting energy for varying α and energy map

Figure B.5. Left: Different paths to the goal starting from x=20 km and y=20 km; Right: Comparison of the initial starting energy for x=20 km and y=20 km

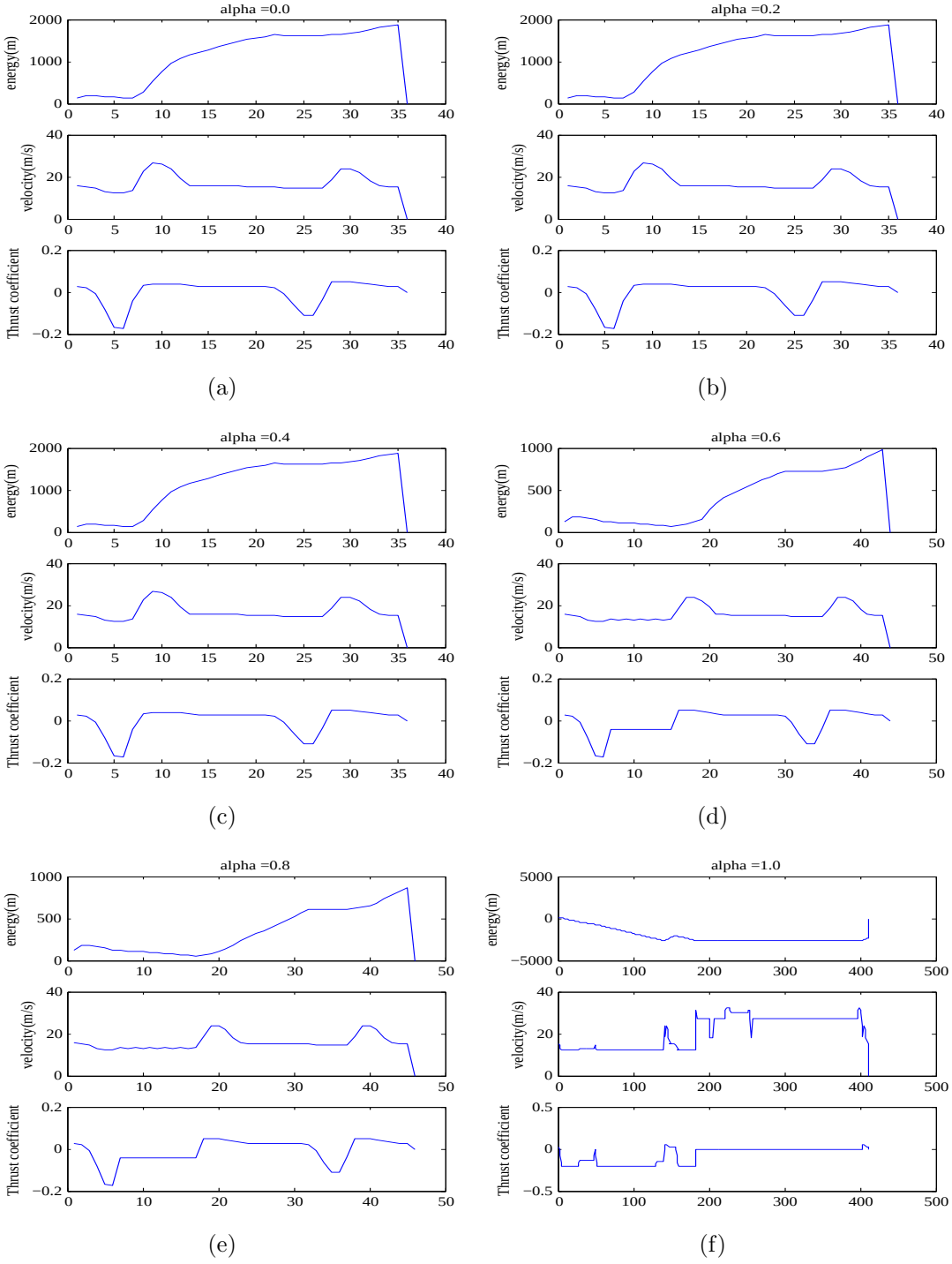

Figure B.6. Energy, Velocity and Thrust Coefficient along the paths for different values of α

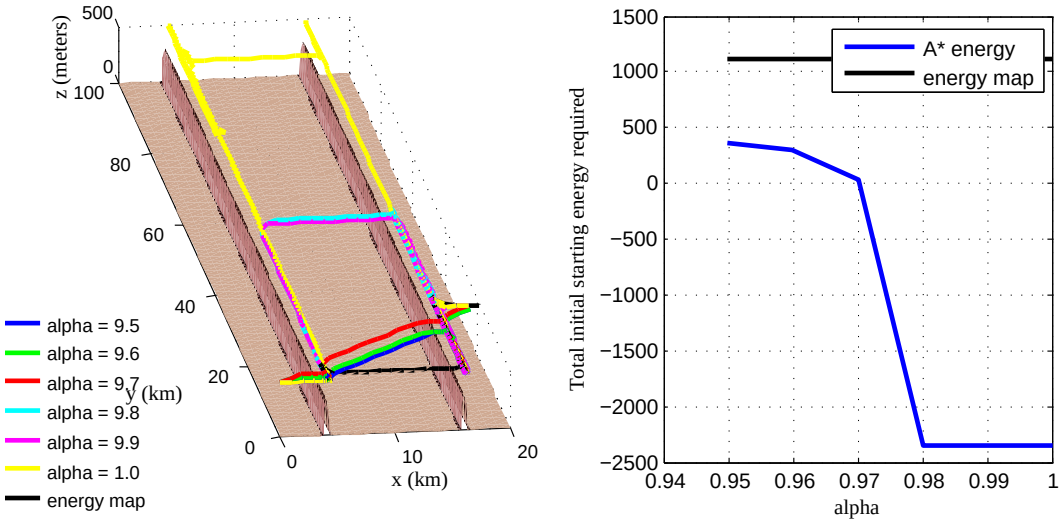

(a) Comparison of A* paths and Energy Map path

(b) Initial Starting energy for varying α and energy map

Figure B.7. Left: Different paths to the goal starting from x=20 km and y=20 km; Right: Comparison of the initial starting energy for x=20 km and y=20 km

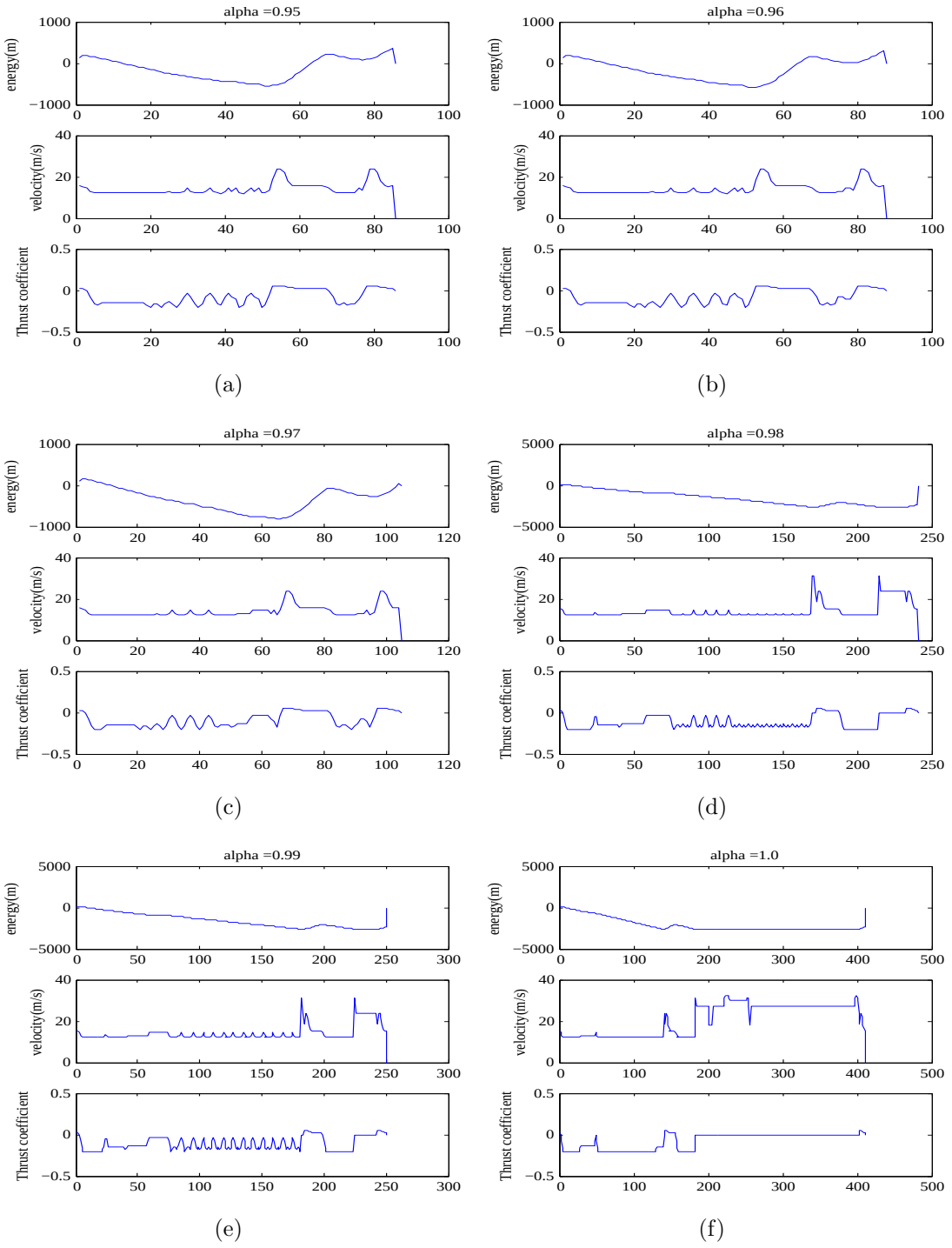

Figure B.8. Energy, Velocity and Thrust Coefficient along the paths for different values of α

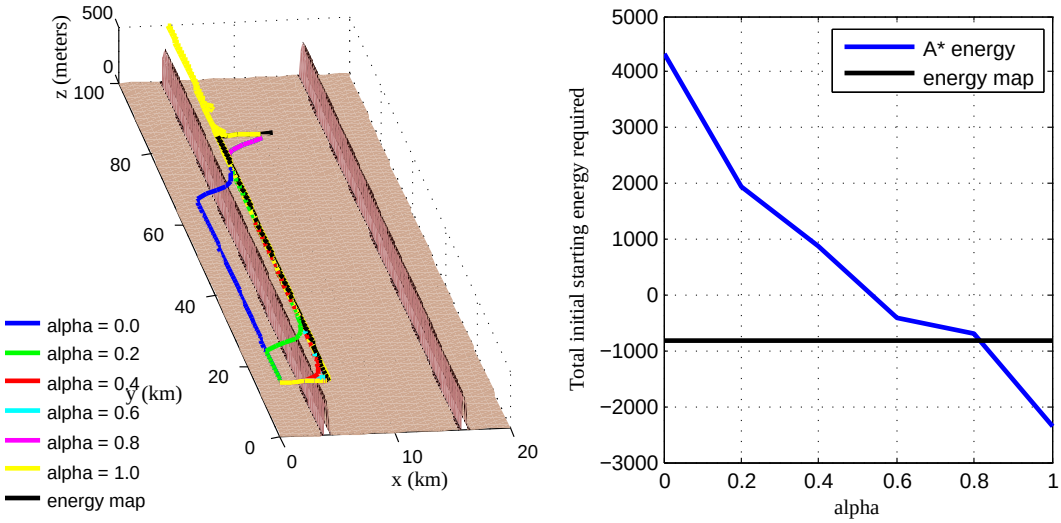

(a) Comparison of A* paths and Energy Map path

(b) Initial Starting energy for varying α and energy map

Figure B.9. Left: Different paths to the goal starting from x=10 km and y=70 km; Right: Comparison of the initial starting energy for x=10 km and y=70 km

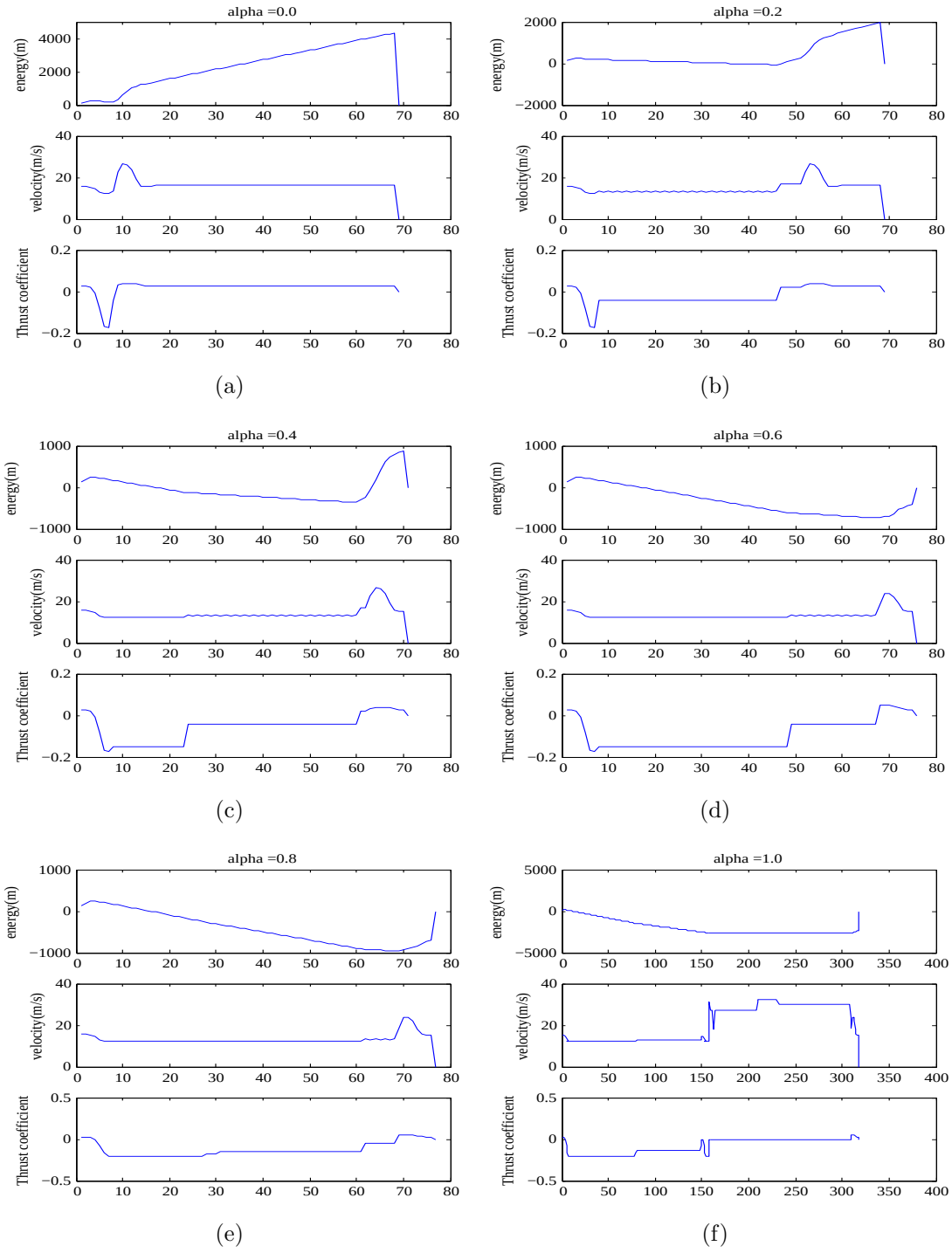

Figure B.10. Energy, Velocity and Thrust Coefficient along the paths for different values of α

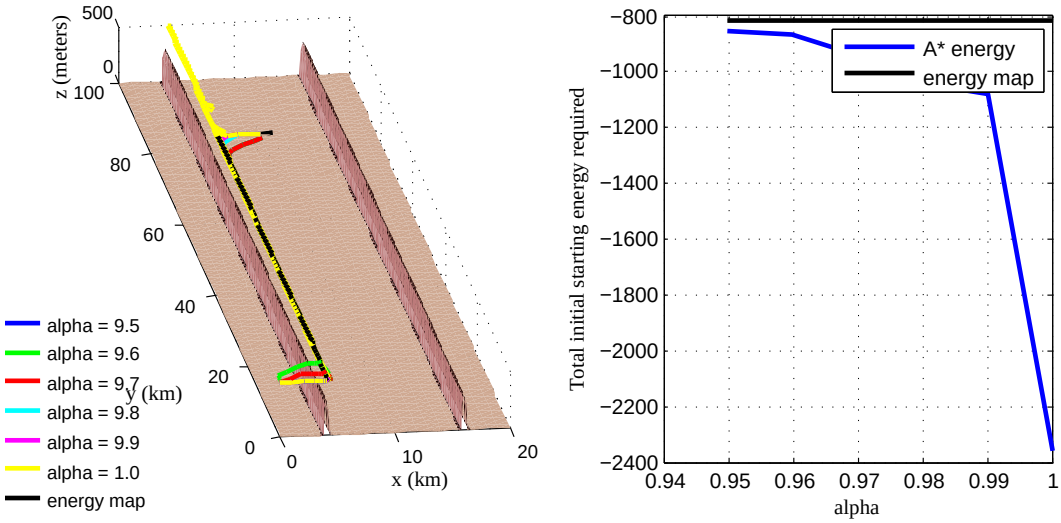

(a) Comparison of A* paths and Energy Map path

(b) Initial Starting energy for varying α and energy map

Figure B.11. Left: Different paths to the goal starting from x=10 km and y=70 km; Right: Comparison of the initial starting energy for x=10 km and y=70 km

Bibliography

[1] Rayleigh, J. W. S. (1883) "The Soaring of Birds," *Nature*, **27**, pp. 534–535.

[2] ——— (1889) "The Sailing Flight of the Albatross," *Nature*, **40**, p. 34.

[3] Boslough, M. B. E. (2002) *Autonomous Dynamic Soaring Platform for Distributed Mobile Sensor Arrays*, *Tech. Rep. SAND2002-1896*, Sandia National Laboratories, Sandia National Laboratories.

[4] Kiceniuk, T. (2001) "Calculations on Soaring in Sink," *Technical Soaring*, **25**(4), pp. 228–230.

[5] Patel, C. K. and I. Kroo (2006) "Control Law Design for Improving UAV Performance using Wind Turbulence," in *AIAA Aerospace Sciences Meeting and Exhibit*, AIAA Paper 2006-0231, American Institute of Aeronautics and Astronautics, Reno, Nevada.

[6] Allen, M. J. (2005) "Autonomous Soaring for Improved Endurance of a Small Uninhabited Air Vehicle," in *43rd AIAA Aerospace Sciences Meeting and Exhibit*, American Institute of Aeronautics and Astronautics, Reno, Nevada.

[7] Allen, M. J. and V. Lin (2007) "Guidance and Control of an Autonomous Soaring Vehicle with Flight Test Results," in *AIAA Aerospace Sciences Meeting and Exhibit*, AIAA Paper 2007-867, American Institute of Aeronautics and Astronautics, Reno, Nevada.
URL `http://dtrs.dfrc.nasa.gov/archive/00001275/`

[8] Edwards, D. J. (2008) "Implementation Details and Flight Test Results of an Autonomous Soaring Controller," in *AIAA Guidance, Navigation and Control Conference*, American Institute of Aeronautics and Astronautics, Reston, Virginia.

[9] Torroella, J. C. R. (2004) *Long Range Evolution-based Path Planning for UAVs through Realistic Weather Environments*, Master's thesis, University of Washington, Seattle, Washington.
URL www.aa.washington.edu/research/afsl/publications/rubio2004thesis.pdf

[10] Jardin, M. R. and A. E. Bryson (2001) "Neighboring Optimal Aircraft Guidance in Winds," *Journal of Guidance, Control and Dynamics*, **24**(4), pp. 710–715.

[11] MacCready Jr., P. B. (1958) "Optimum Airspeed Selector," *Soaring*, pp. 10–11.

[12] Cochrane, J. H. (1999) "MacCready Theory with Uncertain Lift and Limited Altitude," *Technical Soaring*, **23**(3), pp. 88–96.
URL http://faculty.chicagogsb.edu/john.cochrane/research/Papers/newmcred.pdf

[13] Reichmann, H. (1978) *Cross-Country Soaring*, Thomson Publications, Santa Monica, California.

[14] Arho, R. (1974) "Optimal Dolphin Soaring as a Variational Problem," in *OSTIV Publication XIII*, Organisation Scientifique et Technique Internationale du Vol à Voile.

[15] Metzger, D. E. and J. K. Hedrick (1975) "Optimal Flight Paths for Soaring Flight," *Journal of Aircraft*, **12**(11), pp. 867–871.

[16] Sandauer, J. (1978) "Some Problems of the Dolphin-Mode Flight Technique," in *OSTIV Publication XV*, Organisation Scientifique et Technique Internationale du Vol à Voile.

[17] de Jong, J. L. (1981) "The Convex Combination Approach: A Geometric Approach to the Optimization of Sailplane Trajectories," in *OSTIV Publication XVI*, Organisation Scientifique et Technique Internationale du Vol à Voile, pp. 182–201.

[18] Pierson, B. L. and I. Chen (1979) "Minimum Altitude Loss Soaring in a Specified Vertical Wind Distribution," in *NASA Conference Publication 2085, Science and Technology of Low Speed and Motorless Flight* (P. W. Hanson, ed.), NASA, Hampton, Virginia, pp. 305–318.

[19] Sander, G. and F. X. Litt (1979) "On Global Optimal Sailplane Flight Strategy," in *NASA Conference Publication 2085, Science and Technology of Low Speed and Motorless Flight* (P. W. Hanson, ed.), NASA, Hampton, Virginia, pp. 355–376.

[20] "MM5 Community Model Homepage," .
URL `http://www.mmm.ucar.edu/mm5/`

[21] Langelaan, J. W. (2008) "Tree-Based Trajectory Planning to Exploit Atmospheric Energy," in *Proceedings of the American Control Conference*, Seattle, Washington.

[22] ——— (2007) "Long Distance/Duration Trajectories for Small UAVs," in *AIAA Guidance, Navigation and Control Conference*, American Institute of Aeronautics and Astronautics.

[23] Lozano-Perez, T. (1983) "Spatial planning: A configuration space approach," *IEEE transactions on computers*, **100**(32), pp. 108–120.

[24] Lozano-Pérez, T. and M. Wesley (1979) "An algorithm for planning collision-free paths among polyhedral obstacles," *Communications of the ACM*, **22**(10), p. 570.

[25] Tarjan, R. (1971) "Depth-first search and linear grajh algorithms," in *Conference Record 1971 Twelfth Annual Symposium on Switching and Automata Theory*, IEEE, pp. 114–121.

[26] Stentz, A. (1995) "The Focussed D* Algorithm for Real-Time Replanning," in *Proceedings of the International Joint Conference on Artificial Intelligence*.

[27] Anisi, D. A., J. W. C. Robinson, and P. Ogren (2006) "On-line Trajectory Planning for Aerial Vehicles: a Safe Approach with Guaranteed Task Completion," in *AIAA Guidance, Navigation and Control Conference*, AIAA Paper 2006-6107, American Institute of Aeronautics and Astronautics, Keystone, Colorado.

[28] Cormen, T. H., C. E. Leiserson, R. L. Rivest, and C. Stein (2001) *Introduction to Algorithms*, second edition ed., MIT Press, Cambridge, Massachusetts.

[29] MacCready Jr., P. B. (1999) "Regenerative Battery Augmented Soaring (article)," *Journal of Technical Soaring*, **XXIII**(1).

[30] LaValle, S. (2006) *Planning algorithms*, Cambridge Univ Pr.

[31] Chakrabarty, A. and J. W. Langelaan (2009) "Energy Maps for Long-Range Path Planning for Small- and Micro - UAVs," in *AIAA Guidance, Navigation and Control Conference*, AIAA Paper 2009-6113, American Institute of Aeronautics and Astronautics, Chicago, Illinois.

[32] George Young, N. L. S., B. Gaudet and D. R. Stauffer (2009) "Interaction of a mountain lee wave with a basin cold pool," in *13th Conference on Mesoscale Processes*, AMS, American Meteriological Society, Chicago, Illinois.